

SANDIA REPORT

SAND2001-8194
Unlimited Release
Printed March 2001

Influence of Sublimation and Pyrolysis on Quasi-Steady Deflagrations in Confined Porous Energetic Materials

Stephen B. Margolis and Alexander M. Telengator

Prepared by
Sandia National Laboratories
Albuquerque, New Mexico 87185 and Livermore, California 94550

Sandia is a multiprogram laboratory operated by Sandia Corporation,
a Lockheed Martin Company, for the United States Department of
Energy under Contract DE-AC04-94AL85000.

Approved for public release; further dissemination unlimited.



Sandia National Laboratories

Issued by Sandia National Laboratories, operated for the United States Department of Energy by Sandia Corporation.

NOTICE: This report was prepared as an account of work sponsored by an agency of the United States Government. Neither the United States Government, nor any agency thereof, nor any of their employees, nor any of their contractors, subcontractors, or their employees, make any warranty, express or implied, or assume any legal liability or responsibility for the accuracy, completeness, or usefulness of any information, apparatus, product, or process disclosed, or represent that its use would not infringe privately owned rights. Reference herein to any specific commercial product, process, or service by trade name, trademark, manufacturer, or otherwise, does not necessarily constitute or imply its endorsement, recommendation, or favoring by the United States Government, any agency thereof, or any of their contractors or subcontractors. The views and opinions expressed herein do not necessarily state or reflect those of the United States Government, any agency thereof, or any of their contractors.

Printed in the United States of America. This report has been reproduced directly from the best available copy.

Available to DOE and DOE contractors from
U.S. Department of Energy
Office of Scientific and Technical Information
P.O. Box 62
Oak Ridge, TN 37831

Telephone: (865)576-8401
Facsimile: (865)576-5728
E-Mail: reports@adonis.osti.gov
Online ordering: <http://www.doe.gov/bridge>

Available to the public from
U.S. Department of Commerce
National Technical Information Service
5285 Port Royal Rd
Springfield, VA 22161

Telephone: (800)553-6847
Facsimile: (703)605-6900
E-Mail: orders@ntis.fedworld.gov
Online order: <http://www.ntis.gov/ordering.htm>



SAND2001-8194
Unlimited Release
Printed March 2001

INFLUENCE OF SUBLIMATION AND PYROLYSIS ON QUASI-STEADY DEFLAGRATIONS IN CONFINED POROUS ENERGETIC MATERIALS

Stephen B. Margolis[†] and Alexander M. Telengator[‡]

[†]Combustion Research Facility
Sandia National Laboratories
Livermore, California 94551-0969 USA

[‡]Department of Mechanical and Aerospace Engineering
University of California, San Diego
La Jolla, California 92093-0411 USA

Abstract

Deflagrations in porous energetic materials under confinement are generally characterized by a relatively rapid increase in the burning rate as the pressure difference, or overpressure, in the burned-gas region relative to that deep within the pores of the unburned solid increases. Specifically, there appears to be a range of overpressures in which the sensitivity, or slope, of the propagation speed as a function of overpressure transitions from relatively small to large values. This effect has been qualitatively attributed to the fact that a sufficient overpressure reverses the gas flow and thus allows the burned gas to permeate, and therefore preheat, the porous material. However, quantitative descriptions of both the process itself and the corresponding burning-rate dependencies have only recently been achieved. The present work reflects a further refinement in this analytical description in that the melt layer, which underlies several previous studies and is likely to exist only at modest overpressures, is replaced by sublimation and pyrolysis at the material surface, followed by an attached gas flame that converts the unburned gaseous reactants to final products. As a result, gaseous reactants as well as products now permeate the porous solid, thereby affecting the propagation speed significantly and modifying both the combustion-wave structure and the transition to convection-enhanced burning.

This page intentionally left blank.

INFLUENCE OF SUBLIMATION AND PYROLYSIS ON QUASI-STEADY DEFLAGRATIONS IN CONFINED POROUS ENERGETIC MATERIALS

1. Introduction

The nature of combustion in energetic materials has long been of interest in the fields of propulsion and pyrotechnics. More recently, the fact that such materials can undergo significant degradation and develop corresponding levels of porosity has led to the inclusion of important two-phase-flow effects in a number of recent models. These effects become even more significant when, under full or partial confinement, the growing overpressure that develops in the burned-gas region becomes sufficiently high to drive the burned gas into the pores of the unburned solid. This latter phenomenon is known, from numerous experiments on granular materials (*cf.* [1],[2]), to lead to a rapid increase in the burning rate with overpressure. This process is often referred to as a transition from “conductive” to “convective” burning because of the increasingly significant role that convective transport of the hot gas plays, relative to diffusion, in preheating the solid. Nonetheless, the transition to this regime has now been shown theoretically to occur over a range of overpressures in which both diffusion and gas-phase convective transport play non-negligible roles [3]. This transition is a defining characteristic of deflagrations in confined porous materials, and the purpose of the present work is to reconsider this type of problem by introducing several modifications in a previous mathematical model [3] that tend to better reflect the actual combustion-wave structure as the overpressure increases. These modifications, which replace a bubbling melt layer with sublimation and pyrolysis reactions at the material surface, lead to a more direct coupling between the burned gas and porous solid, thereby affecting the resulting expression for the burning rate.

The question of the existence or nonexistence of a melt layer stems from the fact that, depending on the type of energetic material, the deflagration of even nonporous solids is often accompanied by a bubbling melt layer adjacent to the solid surface, with combustion of the liquid reactants producing gas-phase products (*cf.* [4],[5],[6]). This occurs, for example, in the burning of the nitramine HMX at moderate pressures, and was reflected in the previous analysis of the transition regime [3]. However, at more elevated overpressures, such as those that inevitably accompany a confined deflagration, this melt layer tends to disappear, leaving only the solid and gaseous phases to be considered. A reasonable model should, in that case, account for surface pyrolysis, sublimation, and the burning of the resulting gas-phase reactants. While such processes often have been taken into account in the analysis of unconfined, nonporous propellants in the absence of melting (*cf.* [4],[7],[8],[9]), it is reasonable now to extend this type of model to the burning of porous materials under confinement. One consequence of this extension, aside from the more direct burned-gas/porous-solid coupling indicated above, is that the gas-phase component of

the solid/gas region contains not only final gas-phase products, but unburned gas-phase reactants as well. These effects are ultimately reflected in the derived expression of the burning rate, which, as in the case of the previous model, predicts the transition to a convection-driven enhancement of the propagation speed as the overpressure increases.

2. Mathematical Formulation

The present formulation of porous energetic-material combustion in the presence of confinement contains a combination of elements from two different types of models. In the first of these ([4],[8]), sublimation and pyrolysis effects in the absence of melting were considered in the context of an unconfined, nonporous propellant, whereas in the second ([3],[6]), porosity, two-phase-flow and confinement were incorporated into a melting model without the gas-producing solid-phase reactions. Thus, in the present study, we synthesize these various effects by reconsidering the latter problem subject to the overall reaction mechanism $R(s) \rightarrow P(g)$, $R(s) \rightarrow R(g)$, $R(g) \rightarrow P(g)$. The first of these corresponds to direct pyrolysis of the solid material $R(s)$ to final gas-phase products $P(g)$, the second is the sublimation reaction that produces the gas-phase reactants (or intermediates) $R(g)$, and the third is the strictly gas-phase reaction that also produces the final products $P(g)$. The sublimation reaction may be generally taken as endothermic, whereas the pyrolysis and gas-phase reactions are exothermic.

The structure of the one-dimensional (planar) propagating combustion wave is sketched in Figure 1. At the propellant surface, denoted by $\tilde{x} = \tilde{x}_c$, a specified fraction $\beta_c > 0$ of the solid undergoes sublimation, thereby producing the gaseous reactants $R(g)$, while the remainder, $1 - \beta_c$, undergoes pyrolysis to form the gas-phase products $P(g)$. In this work, the gas-phase reaction $R(g) \rightarrow P(g)$ is assumed to occur in a distributed reaction zone in the region $\tilde{x} > \tilde{x}_c$, which is the obvious situation that exists in the nonporous limit ([4],[8]). However, because sufficiently large overpressures can drive the gas flow into the *porous* solid, the location of the distributed gas-phase reaction may, in appropriate parameter regimes, extend into the solid/gas region as well. This is particularly true if the temperature of the gas and solid are not in equilibrium, in which case it is possible for the local gas temperature to exceed that of the solid in the solid/gas region. Thus, in the limit of large reaction activation energies described below, there are potentially several different regimes to consider, depending on whether the thin gas-phase reaction zone lies in the strictly gaseous region $\tilde{x} > \tilde{x}_c$, in the neighborhood $\tilde{x} \approx \tilde{x}_c$, or in the solid/gas region $\tilde{x} < \tilde{x}_c$. In focusing on the first of these regimes, we thus seek to also clarify the influence of overpressure on the gas-flame location as the former increases from zero. To simplify the analysis of this regime, we restrict consideration to the single-temperature limit corresponding to an infinite rate of interphase heat transfer.

Regarding the gas pressure itself, we note that in contrast to the unconfined problem, for

which it is reasonable to assume a constant pressure [6], the gas pressure varies significantly in the solid/gas preheat region [3]. There, the gas velocity is assumed to be related phenomenologically to the pressure gradient according to Darcy's law for flow in porous media. In the purely gaseous region $\tilde{x} > \tilde{x}_c$, however, the gas pressure is assumed to equilibrate sufficiently rapidly on the time scale of interest that it may be taken as independent of \tilde{x} . We shall also ultimately consider the problem to be quasi-steady ([3],[10]). That is, the build-up of pressure due to confinement is assumed to occur on a longer time scale than that associated with the flame structure and, consequently, the pressure for $\tilde{x} > \tilde{x}_c$ may be regarded as constant in the quasi-static sense. The gas density, on the other hand, varies spatially throughout solid/gas and gaseous preheat regions according to the equation of state, approaching its burned value as the overall gas-phase reaction nears completion. The gaseous reactants, which are produced at the solid surface through sublimation, and the gas products, which are produced both by surface pyrolysis and the distributed gas-phase reaction that consumes the gas-phase reactants, are able to permeate into the unburned region through both diffusion and pressure-driven convection.

In the mathematical description that follows, both solid- and gas-phase reactions are assumed to be Arrhenius in nature, with large activation energies that are of the same order of magnitude. The deflagration wave, which propagates from right to left, thus converts the solid energetic material into gaseous products. Although the fact that the problem is confined renders it inherently nonsteady, we assume, as indicated in the previous remarks with respect to the gas pressure, that the confining boundaries are sufficiently remote relative to the spatial scale of the combustion wave that conditions at appropriately large values of $|\tilde{x}|$ are quasi-static. In this regime, the problem may thus be considered as quasi-steady and infinite, ultimately allowing the calculation of a well-defined burning rate as a function of the (quasi-static) pressure difference, or overpressure, between that of the completely burned gas and that of the pores deep within the unburned porous solid. This overpressure represents the effect of confinement in the present burning regime and leads to the aforementioned reversal of the gas flow into the pores of the unburned solid. For weak permeabilities, this gas permeation into the solid/gas region exhibits a boundary-layer structure with respect to the gas velocity and pressure [3]. Consequently, for weak permeabilities and large activation energies, the combustion-wave structure considered here consists of five identifiable regions. From left to right, these include a solid/gas preheat zone, a thin gas-permeation boundary layer within the solid/gas region adjacent to the solid surface at which sublimation and pyrolysis occur, a gas preheat region, an even thinner (for large activation energies) gas-phase reaction zone (or chemical boundary layer) in which the gaseous reactants are converted into burned products, and finally, the burned-gas region. The fact that the overpressure tends to drive at least some of the gas in the direction of the unburned solid implies that both the final gas products as well as the gaseous reactants produced by sublimation will exist within the solid/gas region, and therefore the solution will be a function of the specified mixture ratio at $\tilde{x} = -\infty$.

Denoting solid- and gas-phase quantities by the subscripts “s” and “g”, respectively, gas-phase mass conservation may be specified in dimensional form (denoted by tildes) as

$$\frac{\partial}{\partial \tilde{t}} (\tilde{\rho}_g Y) + \frac{\partial}{\partial \tilde{x}} (\tilde{\rho}_g \tilde{u}_g Y) = \frac{\partial}{\partial \tilde{x}} \left(\tilde{\rho}_g \tilde{D} \frac{\partial Y}{\partial \tilde{x}} \right), \quad \tilde{x} < \tilde{x}_c, \quad (1)$$

$$\frac{\partial}{\partial \tilde{t}} (\tilde{\rho}_g Y) + \frac{\partial}{\partial \tilde{x}} (\tilde{\rho}_g \tilde{u}_g Y) - \frac{\partial}{\partial \tilde{x}} \left(\tilde{\rho}_g \tilde{D} \frac{\partial Y}{\partial \tilde{x}} \right) = -\tilde{A}_g (\tilde{\rho}_g Y)^n \exp \left(-\tilde{E}_g / \tilde{R}^\circ \tilde{T} \right), \quad \tilde{x} > \tilde{x}_c, \quad (2)$$

where Y is the mass fraction of gas-phase reactants. In addition, the gas-phase volume fraction α is equal to the porosity α_s (assumed constant) in the solid/gas region $\tilde{x} < \tilde{x}_c$, and is identically equal to unity in the purely gaseous region $\tilde{x} > \tilde{x}_c$. The remaining variables in Eqs. (1) and (2) are the temporal and spatial coordinates \tilde{t} and \tilde{x} , the temperature \tilde{T} , and the gas density $\tilde{\rho}_g$ and velocity \tilde{u}_g . Other quantities that appear are the gas constant \tilde{R}° , the Arrhenius prefactor \tilde{A}_g and the overall activation-energy \tilde{E}_g of the gas-phase reaction, the reaction order n , and the mass diffusivity \tilde{D} of the gaseous species. Mass conservation in the solid phase is identically satisfied since the solid is assumed to have a constant density $\tilde{\rho}_s$ and zero velocity, while overall gas-phase mass continuity is given for all \tilde{x} by

$$\frac{\partial \tilde{\rho}_g}{\partial \tilde{t}} + \frac{\partial}{\partial \tilde{x}_3} (\tilde{\rho}_g \tilde{u}_g) = 0, \quad \tilde{x} \neq \tilde{x}_c. \quad (3)$$

The corresponding energy-conservation equations in the regions $\tilde{x} < \tilde{x}_c$ and $\tilde{x} > \tilde{x}_c$ are given by

$$\begin{aligned} \frac{\partial}{\partial \tilde{t}} \left[\tilde{\rho}_s \tilde{c}_s (1 - \alpha_s) \tilde{T} + \tilde{\rho}_g \tilde{c}_g \alpha_s \tilde{T} \right] + \frac{\partial}{\partial \tilde{x}} \left(\tilde{\rho}_g \tilde{c}_g \tilde{u}_g \alpha_s \tilde{T} \right) \\ = \frac{\partial}{\partial \tilde{x}} \left\{ \left[\tilde{\lambda}_s (1 - \alpha_s) + \tilde{\lambda}_g \alpha_s \right] \frac{\partial \tilde{T}}{\partial \tilde{x}} \right\} + \alpha_s \frac{\partial \tilde{p}_g}{\partial \tilde{t}}, \quad \tilde{x} < \tilde{x}_c, \end{aligned} \quad (4)$$

$$\begin{aligned} \frac{\partial}{\partial \tilde{t}} \left(\tilde{\rho}_g \tilde{c}_g \tilde{T} \right) + \frac{\partial}{\partial \tilde{x}} \left(\tilde{\rho}_g \tilde{c}_g \tilde{u}_g \tilde{T} \right) = \frac{\partial}{\partial \tilde{x}} \left(\tilde{\lambda}_g \frac{\partial \tilde{T}}{\partial \tilde{x}} \right) \\ + (\tilde{Q} + \tilde{\gamma}_s) \tilde{A}_g (\tilde{\rho}_g Y)^n \exp \left(-\tilde{E}_g / \tilde{R}^\circ \tilde{T} \right) + \frac{\partial \tilde{p}_g}{\partial \tilde{t}}, \quad \tilde{x} > \tilde{x}_c, \end{aligned} \quad (5)$$

where Eq. (4) represents the overall energy-conservation equation in the solid/gas region and p_g is the gas-pressure variable. Other quantities appearing in Eqs. (4) and (5) include \tilde{c} and $\tilde{\lambda}$, which denote heat capacity and thermal conductivity respectively, $\tilde{\gamma}_s$, the solid-propellant heat of sublimation, and \tilde{Q} , which represents the overall gaseous heat of reaction. The latter two quantities are evaluated at $\tilde{T} = 0$, and positive values of $\tilde{\gamma}_s$ imply endothermicity. Using Eq. (2), the reaction-rate term in Eq. (4) may be eliminated, allowing the energy equation in the gaseous region to be rewritten as

$$\begin{aligned} \frac{\partial}{\partial \tilde{t}} \left[\tilde{\rho}_g \tilde{c}_g \tilde{T} + (\tilde{Q} + \tilde{\gamma}_s) \tilde{\rho}_g Y \right] + \frac{\partial}{\partial \tilde{x}} \left[\tilde{\rho}_g \tilde{c}_g \tilde{u}_g \tilde{T} + (\tilde{Q} + \tilde{\gamma}_s) \tilde{\rho}_g \tilde{u}_g Y \right] \\ = \frac{\partial}{\partial \tilde{x}} \left[\tilde{\lambda}_g \frac{\partial \tilde{T}}{\partial \tilde{x}} + (\tilde{Q} + \tilde{\gamma}_s) \tilde{\rho}_g \tilde{D} \frac{\partial Y}{\partial \tilde{x}} \right] + \frac{\partial \tilde{p}_g}{\partial \tilde{t}} \quad \tilde{x} > \tilde{x}_c. \end{aligned} \quad (5')$$

With respect to momentum conservation, we adopt simplifications similar to those introduced previously for this type of problem [3]. In particular, assuming that the Mach number is small, we approximate the gas pressure in the gaseous region $\tilde{x} > x_c$ as homogeneous, and hence constant in the quasi-steady sense, as discussed above. In the region $\tilde{x} < \tilde{x}_c$, however, there is a drag on the gas as it flows through the porous solid. This is modeled by adopting Darcy's law for flow in a porous medium and thus, in place of momentum conservation, we have the conditions

$$\tilde{u}_g = -\frac{\tilde{\kappa}(\alpha_s)}{\alpha_s \tilde{\mu}_g} \frac{\partial \tilde{p}_g}{\partial \tilde{x}}, \quad x < \tilde{x}_c; \quad \tilde{p}_g = \tilde{p}_g^b, \quad \tilde{x} > \tilde{x}_c, \quad (6)$$

where $\tilde{\kappa}$ and $\tilde{\mu}_g$ are the permeability of the solid/gas region and the gas-phase viscosity, respectively, and p_g^b is the quasi-steady pressure in the burned-gas region. The above system of equations is closed by including the gas-phase equation of state, assumed to be that of an ideal gas, given by

$$\tilde{p}_g = \tilde{\rho}_g \left(\frac{Y}{\tilde{W}_R} + \frac{1-Y}{\tilde{W}_P} \right) R^\circ \tilde{T}, \quad (7)$$

where \tilde{W}_R and \tilde{W}_P are the respective molecular weights of the gas reactants and products.

The set of equations (1) – (7) for \tilde{T} , \tilde{Y} , \tilde{u}_g , \tilde{p}_g and $\tilde{\rho}_g$ is complemented by boundary conditions at $\tilde{x} = \pm\infty$ and jump/continuity conditions at the material surface $\tilde{x} = \tilde{x}_c$. Denoting unburned and burned values by subscripts/superscripts “*u*” and “*b*”, respectively, and values at the material surface by the subscript “*c*”, the former conditions are given by

$$\tilde{u}_g \rightarrow \tilde{u}_g^b, \quad \tilde{T} \rightarrow \tilde{T}_b, \quad Y \rightarrow 0 \quad \text{as } \tilde{x} \rightarrow +\infty, \quad (8)$$

$$\tilde{u}_g \rightarrow 0, \quad \tilde{T} \rightarrow \tilde{T}_u, \quad \tilde{p}_g \rightarrow \tilde{p}_g^u, \quad Y \rightarrow \phi \quad \text{as } \tilde{x} \rightarrow -\infty, \quad (9)$$

where $0 \leq \phi \leq 1$ is the specified mass fraction of gaseous reactants deep within the porous solid. We note that the burned temperature \tilde{T}_b and gas velocity \tilde{u}_g^b are to be determined.

At the material surface, the sublimation/pyrolysis reaction that produces both gas-phase reactants and products is assumed, like the distributed gas-phase reaction, to be Arrhenius in nature with a large activation energy \tilde{E}_s that is of the same order of magnitude as \tilde{E}_g . Thus, the (unknown) rate of regression $-d\tilde{x}_c/d\tilde{t}$ of the solid surface is related to the (unknown) surface temperature \tilde{T}_c according to

$$-\tilde{\rho}_s \frac{d\tilde{x}_c}{d\tilde{t}} = \tilde{A}_s \exp\left(-\tilde{E}_s/\tilde{R}^\circ \tilde{T}_c\right), \quad (10)$$

where \tilde{A}_s is the exponential reciprocal-time prefactor of the surface reaction. In addition, we have the continuity conditions

$$\tilde{p}_g|_{\tilde{x}=\tilde{x}_c^-} = \tilde{p}_g|_{\tilde{x}=\tilde{x}_c^+} = \tilde{p}_g^b, \quad \tilde{T}|_{\tilde{x}=\tilde{x}_c^-} = \tilde{T}|_{\tilde{x}=\tilde{x}_c^+} = \tilde{T}_c, \quad Y|_{\tilde{x}=\tilde{x}_c^-} = Y|_{\tilde{x}=\tilde{x}_c^+} = Y_c, \quad (11)$$

where the mass fraction of the gaseous reactant at the solid surface, Y_c , is to be determined as well. Finally, continuity of overall mass flux, reactant mass flux and total enthalpy flux across the surface $\tilde{x} = \tilde{x}_c$ imply the jump conditions

$$\tilde{u}_g|_{\tilde{x}=\tilde{x}_c^+} - \alpha_s \tilde{u}_g|_{\tilde{x}=\tilde{x}_c^-} = (1 - \alpha_s) \frac{d\tilde{x}_c}{d\tilde{t}} \left(1 - \frac{\tilde{\rho}_s}{\tilde{\rho}_g^c} \right), \quad (12)$$

$$\tilde{\rho}_g^c \tilde{D} \frac{dY}{d\tilde{x}} \Big|_{\tilde{x}=\tilde{x}_c^+} - \alpha_s \tilde{\rho}_g^c \tilde{D} \frac{dY}{d\tilde{x}} \Big|_{\tilde{x}=\tilde{x}_c^-} = (1 - \alpha_s) \tilde{\rho}_s \frac{d\tilde{x}_c}{d\tilde{t}} (\beta_c - Y_c), \quad (13)$$

and

$$\begin{aligned} \tilde{\lambda}_g \frac{d\tilde{T}}{d\tilde{x}} \Big|_{\tilde{x}=\tilde{x}_c^+} - \left[(1 - \alpha_s) \tilde{\lambda}_s + \alpha_s \tilde{\lambda}_g \right] \frac{d\tilde{T}}{d\tilde{x}} \Big|_{\tilde{x}=\tilde{x}_c^-} \\ = (1 - \alpha_s) \tilde{\rho}_s \frac{d\tilde{x}_c}{d\tilde{t}} \left[(\tilde{c}_s - \tilde{c}_g) \tilde{T}_c + (1 - \beta_c) \tilde{Q} - \beta_c \tilde{\gamma}_s \right], \end{aligned} \quad (14)$$

where $\tilde{\rho}_g^c = \tilde{\rho}_g|_{\tilde{x}=\tilde{x}_c}$ and β_c is the fraction of propellant that undergoes sublimation to gaseous reactants (as opposed to undergoing pyrolysis to gaseous products) via the surface reaction at $\tilde{x} = \tilde{x}_c$. We note that Eq. (12) was used in obtaining the final form of Eqs. (13) and (14). We observe that whereas Eqs. (13) and (14) imply a discontinuity in $dY/d\tilde{x}$ and $d\tilde{T}/d\tilde{x}$, Eq. (12) indicates a jump in the variable \tilde{u}_g itself at $\tilde{x} = x_c$ due to the conversion of the solid material to gaseous species there.

3. Dimensionless Form of the Quasi-Steady Problem

Confining attention to quasi-steady solutions of the preceding problem, we primarily seek to determine the propagation speed $\tilde{U} = -d\tilde{x}_c/d\tilde{t}$ as a function of the overpressure $\tilde{p}_g^b - \tilde{p}_g^u$ and other parameters. Regarding \tilde{U} as a characteristic velocity, and assuming constant values for the thermal conductivities and heat capacities, it is convenient to first cast the problem in dimensionless form by introducing the nondimensional variables

$$x = \frac{\tilde{\rho}_s \tilde{c}_s \tilde{U}}{\tilde{\lambda}_s} \tilde{x}, \quad t = \frac{\tilde{\rho}_s \tilde{c}_s \tilde{U}^2}{\tilde{\lambda}_s} \tilde{t}, \quad T = \frac{\tilde{T}}{\tilde{T}_u}, \quad u_g = \frac{\tilde{u}_g}{\tilde{U}}, \quad \rho_g = \frac{\tilde{\rho}_g}{\tilde{\rho}_g^u}, \quad p_g = \frac{\tilde{p}_g}{\tilde{p}_g^u}, \quad (15)$$

where the upstream reference gas density, based on the equation of state (7) evaluated at $x \rightarrow -\infty$, is defined as

$$\tilde{\rho}_g^u = \frac{\tilde{p}_g^u}{\tilde{R}^\circ \tilde{T}_u} \left(\frac{\phi}{\tilde{W}_R} + \frac{1 - \phi}{\tilde{W}_P} \right)^{-1}. \quad (16)$$

We also introduce nondimensional parameters and the burning-rate eigenvalue, which are defined as

$$\begin{aligned} w = \frac{\tilde{W}_R}{\tilde{W}_P}, \quad \bar{\phi} = \phi + w(1 - \phi), \quad Le = \frac{\tilde{\lambda}_g}{\tilde{\rho}_g \tilde{c}_g \tilde{D}}, \quad \hat{r} = \frac{\tilde{\rho}_g^u}{\tilde{\rho}_s}, \quad \hat{l} = \frac{\tilde{\lambda}_g}{\tilde{\lambda}_s}, \quad \hat{b} = \frac{\tilde{c}_g}{\tilde{c}_s}, \\ \gamma_s = \frac{\tilde{\gamma}_s}{\tilde{c}_s \tilde{T}_u}, \quad Q = \frac{\tilde{Q}}{\tilde{c}_s \tilde{T}_u}, \quad \kappa = \frac{\tilde{\rho}_s \tilde{c}_s \tilde{p}_g^u \tilde{\kappa}(\alpha_s)}{\tilde{\lambda}_s \tilde{\mu}_g}, \quad \chi = \frac{\gamma - 1}{\gamma}, \quad \hat{\pi} = \frac{\tilde{p}_g^u}{\tilde{\rho}_s \tilde{c}_s \tilde{T}_u} = \hat{r} \hat{b} \chi, \\ N_s = \frac{\tilde{E}_s}{\tilde{R}^\circ \tilde{T}_c}, \quad \Lambda_s = \frac{\tilde{A}_s}{\tilde{\rho}_s \tilde{U}} e^{-N_s}, \quad N_g = \frac{\tilde{E}_g}{\tilde{R}^\circ \tilde{T}_b}, \quad \Lambda_g = \frac{\tilde{\lambda}_s \tilde{A}_g (\tilde{\rho}_g^u)^n}{\tilde{\rho}_s^2 \tilde{c}_s \tilde{U}^2} e^{-N_g}, \end{aligned} \quad (17)$$

where γ is the ratio of specific heats for the gas phase and Le is the gas-phase Lewis number. The latter is considered constant based on the assumption that both $\tilde{\lambda}_g$ and $\tilde{\rho}_g \tilde{D}$ are constant as well. The quantity Λ_g is the burning-rate eigenvalue, since its determination will yield, according to its definition, an expression for the dimensional burning rate \tilde{U} . The related quantity Λ_s , on the other hand, depends on both \tilde{U} and the unknown surface temperature \tilde{T}_c through the definition of N_s . Consequently, determination of Λ_s , which may be regarded as a surface-temperature eigenvalue, will yield, once Λ_g is known, an expression for T_c in terms of \tilde{U} according to the relationship

$$\Lambda_s^2 = \Lambda_g \frac{\tilde{A}_s^2 \tilde{c}_s}{\tilde{A}_g \tilde{\lambda}_s (\tilde{\rho}_g^u)^n} e^{-(2N_s - N_g)}. \quad (18)$$

Since the nondimensional propagation speed, by definition, is equal to unity, it is convenient to analyze the problem in terms of the moving coordinate $\xi = x + t$ whose origin is defined to be x_c . In this coordinate system, the steadily-propagating combustion wave is time-independent, and its solution is thus determined, upon substitution of the definitions given above, as the solution of the nondimensional problem

$$\frac{d}{d\xi} [\rho_g(u_g + 1)] = 0, \quad \xi \neq 0, \quad (19)$$

$$\frac{d}{d\xi} [\hat{r} \rho_g Y(u_g + 1)] = \frac{\hat{l}}{\hat{b}} Le^{-1} \frac{d^2 Y}{d\xi^2}, \quad \xi < 0, \quad (20)$$

$$\frac{d}{d\xi} [\hat{r} \rho_g Y(u_g + 1)] = \frac{\hat{l}}{\hat{b}} Le^{-1} \frac{d^2 Y}{d\xi^2} - \Lambda_g (\rho_g Y)^n \exp \left[N_g \left(1 - \frac{T_b}{T} \right) \right], \quad \xi > 0, \quad (21)$$

$$(1 - \alpha_s) \frac{dT}{d\xi} + \hat{r} \hat{b} \alpha_s \frac{d}{d\xi} [\rho_g(u_g + 1)T] = \frac{d}{d\xi} \left[(1 - \alpha_s + \hat{l} \alpha_s) \frac{dT}{d\xi} \right] + \hat{\pi} \alpha_s \frac{dp_g}{d\xi}, \quad \xi < 0, \quad (22)$$

$$\frac{d}{d\xi} \left\{ \hat{r} \rho_g(u_g + 1) [\hat{b}T + (Q + \gamma_s)Y] \right\} = \frac{d}{d\xi} \left[\hat{l} \frac{dT}{d\xi} + (Q + \gamma_s) \frac{\hat{l}}{\hat{b}} Le^{-1} \frac{dY}{d\xi} \right], \quad \xi > 0, \quad (23)$$

$$u_g = -\frac{\kappa(\alpha_s)}{\alpha_s} \frac{dp_g}{d\xi}, \quad \xi < 0, \quad (24)$$

$$\rho_g T [Y + w(1 - Y)] = p_g \bar{\phi}, \quad (25)$$

subject to the boundary conditions

$$u_g \rightarrow 0, \quad T \rightarrow 1, \quad p_g \rightarrow 1, \quad Y \rightarrow \phi \quad \text{as} \quad \xi \rightarrow -\infty, \quad (26)$$

$$p_g = p_g^b \quad \text{for} \quad \xi > 0; \quad u_g \rightarrow u_g^b, \quad T \rightarrow T_b, \quad Y \rightarrow 0 \quad \text{as} \quad \xi \rightarrow +\infty, \quad (27)$$

and the material-surface conditions at $\xi = 0$, which are now given by

$$p_g|_{\xi=0^-} = p_g|_{\xi=0^+} = p_g^b, \quad T|_{\xi=0^-} = T|_{\xi=0^+} = T_c, \quad Y|_{\xi=0^-} = Y|_{\xi=0^+} = Y_c, \quad (28)$$

$$u_g|_{\xi=0^+} - \alpha_s u_g|_{\xi=0^-} = (1 - \alpha_s) \left(\frac{1}{\hat{r}\rho_g^c} - 1 \right), \quad (29)$$

$$\frac{dY}{d\xi}|_{\xi=0^+} - \alpha_s \frac{dY}{d\xi}|_{\xi=0^-} = (1 - \alpha_s) \frac{\hat{b}}{\hat{l}} Le (Y_c - \beta_c), \quad (30)$$

$$\hat{l} \frac{dT}{d\xi}|_{\xi=0^+} - (1 - \alpha_s + \hat{l}\alpha_s) \frac{dT}{d\xi}|_{\xi=0^-} = (1 - \alpha_s) \left[(\hat{b} - 1)T_c - (1 - \beta_c)Q + \beta_c\gamma_s \right], \quad (31)$$

where, from the equation of state, $\rho_g^c = (p_g^b \bar{\phi} / T_c) [Y_c + w(1 - Y_c)]^{-1}$. Finally, from Eq. (10) and the definition of Λ_s in Eqs. (17), we have

$$\Lambda_s = 1. \quad (32)$$

which, from the relation (18), leads to an expression for T_c through the definition of N_s once Λ_g is known. Equations (19) – (32), which are analyzed below, constitute the complete quasi-steady, planar description of the present problem.

4. Preliminary Analysis

As in a previous study [3], several first integrals of the equation set given above can be performed in order to determine both the burned temperature T_b and the burned-gas velocity u_g^b . In particular, the overall continuity equation (19) is readily integrated in the solid/gas region $\xi < 0$ to obtain

$$\rho_g(u_g + 1) = 1, \quad \xi < 0, \quad (33)$$

where the boundary conditions (26) have been used to evaluate the constant of integration. Solving the equation of state (25) for ρ_g and substituting the result into Eq. (33) then gives the relation

$$u_g + 1 = \frac{T}{\bar{\phi} p_g} [Y + w(1 - Y)], \quad \xi < 0, \quad (34)$$

and thus

$$u_g|_{\xi=0^-} = \frac{T_c}{\bar{\phi} p_g^b} [Y_c + w(1 - Y_c)] - 1. \quad (35)$$

Similarly, Eq. (19) may be integrated in the gaseous region $\xi > 0$, where the constant of integration may be determined by evaluating the result at $\xi = 0^+$ using the previous result (35), the jump condition (29), and the fact that $p_g = p_g^b$ for $\xi \geq 0$. Consequently, we obtain in the gaseous region

$$\rho_g(u_g + 1) = \frac{1}{\hat{r}} (1 - \alpha_s + \hat{r}\alpha_s), \quad (36a)$$

or equivalently,

$$u_g + 1 = (1 - \alpha_s + \hat{r}\alpha_s) \frac{T}{\hat{r}\bar{\phi} p_g^b} [Y + w(1 - Y)], \quad \xi > 0. \quad (36b)$$

Upon evaluation at $\xi \rightarrow +\infty$, this result then provides a relationship between the burned gas velocity u_g^b and the burned temperature T_b as

$$u_g^b = (1 - \alpha_s + \hat{r}\alpha_s) \frac{T_b w}{\hat{r}\phi p_g^b} - 1. \quad (37)$$

Turning attention to the mass continuity and energy equations, Eq. (34) for u_g and the boundary conditions (26) can be used to obtain first integrals of Eqs. (20) and (22) in the region $\xi < 0$ as

$$Y - \phi = \frac{\hat{l}}{\hat{r}\hat{b}} L e^{-1} \frac{dY}{d\xi}, \quad \xi < 0, \quad (38)$$

$$(1 - \alpha_s + \hat{r}\hat{b}\alpha_s)(T - 1) = (1 - \alpha_s + \hat{l}\alpha_s) \frac{dT}{d\xi} + \hat{r}\hat{b}\chi\alpha_s(p_g - 1), \quad \xi < 0. \quad (39)$$

Similarly, integrating Eq. (23) in the region $\xi > 0$ gives, with the aid of Eqs. (27) and (36), the first integral

$$(1 - \alpha_s + \hat{r}\alpha_s)[\hat{b}(T - T_b) + (Q + \gamma_s)Y] = \hat{l} \frac{dT}{d\xi} + (Q + \gamma_s) \frac{\hat{l}}{\hat{b}} L e^{-1} \frac{dY}{d\xi}, \quad \xi > 0. \quad (40)$$

At this point, we subtract Eq. (39) evaluated at $\xi = 0^-$ from Eq. (40) evaluated at $\xi = 0^+$. Using Eq. (38) along with the jump conditions (30) and (31), we thus obtain an expression for the burned temperature T_b as

$$T_b = \frac{(1 - \alpha_s)(Q + 1) + \hat{r}\alpha_s \left\{ (Q + \gamma_s)\phi + \hat{b}[\chi(p_g^b - 1) + 1] \right\}}{\hat{b}(1 - \alpha_s + \hat{r}\alpha_s)}. \quad (41)$$

This result, in turn, can be substituted into Eq. (37) to yield an expression for the burned gas velocity u_g^b , which is given by

$$u_g^b = \frac{w}{\hat{r}\hat{b}p_g^b\bar{\phi}} \left[(1 - \alpha_s)(Q + 1) + \hat{r}\alpha_s \left\{ (Q + \gamma_s)\phi + \hat{b}[\chi(p_g^b - 1) + 1] \right\} \right] - 1. \quad (42)$$

We observe that in the nonporous limit $\alpha_s \rightarrow 0$, the expression for T_b collapses to the standard result $T_b = (Q + 1)/\hat{b}$ for solid-propellant deflagration in the absence of porosity (*cf.* [4],[8]). On the other hand, for porous materials in the limit $\phi \rightarrow 0$, in which case only gas-phase products are present at $\xi = -\infty$, the expressions for both T_b and u_g^b essentially collapse to those that are obtained for an alternative model of the present problem in which there is melting of the solid, rather than sublimation and pyrolysis, at the material surface [3].

The significant effects of porosity, confinement and the presence of gas-phase reactants ($\phi \neq 0$) deep within the porous solid are exhibited in Figures 2a and 2b, where T_b is plotted against the overpressure $p_g^b - 1$ for various values of ϕ and two different values of porosity α_s . From these plots we observe that in the nonporous limit $\alpha_s = 0$, the burned temperature does not depend on

either p_g^b or ϕ , as illustrated by the horizontal line $T_b = T_b^0 = (Q + 1)/\hat{b}$. For nonzero porosities, however, significant modifications that arise from the effects of two-phase flow, the gas-phase pressure difference (overpressure) across the combustion wave and the composition of the gaseous mixture deep within the solid/gas region are evident. In particular, at low overpressures the burned temperature is smaller, especially for smaller values of ϕ , than in the nonporous limit, since some of the heat of reaction must be used to heat the gas within the porous solid. However, this effect diminishes and can even reverse itself with increasing ϕ because, for larger values of ϕ , a greater fraction of the gas within the pores consists of reactants, rather than products. These reactants then ultimately contribute to the overall exothermicity of the deflagration, whereas the gas products within the pores cannot.

An even more significant effect is associated with increasing overpressure, which, as described below, can lead to permeation of the hot gases into the pores of the unburned solid, thereby providing a preheating effect. Indeed, as can be seen in Figures 2a and 2b and from Eq. (41) directly, there is a linear relationship between T_b and $p_g^b - 1$. Consequently, there is generally (provided $T_b < T_b^0$ at zero overpressure) a critical value of overpressure, independent of $\alpha_s > 0$ and given by

$$p_g^b - 1 = \frac{1}{\chi} \left[T_b^0(1 - \phi) - 1 + \phi \frac{1 - \gamma_s}{\hat{b}} \right], \quad (43)$$

at which the burned temperature of the porous problem is the same as that of the nonporous one. The influence of overpressure becomes more pronounced as α_s increases, as reflected in the greater sensitivity (steeper slope) of T_b with respect to $p_g^b - 1$ for larger porosities. This increase in T_b with increasing overpressure will be shown to lead to a corresponding rapid increase in the burning rate that is reflective of a well-known transition to a convection-enhanced mode of burning. Usually referred to simply as “convective” burning, this regime reflects the significance of the pressure-driven permeation of the burned gas into the pores of the unburned material. (*cf.* [2]).

The burned-gas velocity u_g^b , given by Eq. (42), is shown plotted against overpressure for several values of ϕ in Figures 3a and 3b, where the two figures reflect different values of the molecular-weight ratio w . As would be expected, u_g^b , which is initially positive, decreases with increasing overpressure, ultimately becoming negative for values of overpressure beyond the critical value

$$p_g^b - 1 = \frac{1}{1 - \alpha_s \chi - \phi(w - 1)/w} \left[\frac{1}{\hat{r}}(1 - \alpha_s)(T_b^0 - \hat{r}) + \alpha_s \phi \left(T_b^0 + \frac{\gamma_s - 1}{\hat{b}} \right) + \phi \frac{w - 1}{w} \right]. \quad (44)$$

That is, sufficiently large overpressures are capable of reversing the direction of gas flow in the burned region towards the unburned material. The gas velocity just inside the material, $u_g(0^-)$, on the other hand, can be turned negative at substantially lower values of overpressure. However, the critical value of overpressure at which this occurs depends, according to Eq. (35), on the as-yet-unknown values of T_c and Y_c .

According to Eq. (37), the expression for u_g^b depends, in addition to p_g^b , on both ϕ and w , as can be seen in Figures 3a and 3b. To a first approximation, assuming the unburned gas-to-solid density ratio \hat{r} is relatively small, this dependency is proportional to $w/\bar{\phi} = [1 - \phi(w-1)/w]^{-1}$. Thus, for $w \lesssim 1$, u_g^b decreases with increasing ϕ as illustrated in Figure 3a, whereas the opposite trend is observed for $w \gtrsim 1$, as can be seen in Figure 3b. Since it is more likely that the molecular weight of the gaseous reactants exceeds that of the products (*i.e.*, $w > 1$), Figure 3b depicts the more realistic trend. In either case, however, the influences of the gas composition and the molecular-weight ratio on u_g^b diminish in absolute terms as the overpressure increases, reflecting the primarily inverse relationship between u_g^b and p_g^b .

5. The Asymptotic Limit and the Outer Solution

In order to determine the burning-rate eigenvalue, it is necessary to complete the analysis in the gaseous region $\xi > 0$. Equations (21) and (40) constitute a closed system of two equations for Y and T in that region, since u_g and ρ_g are given in terms of these variables by Eqs. (25) and (36), respectively. In order to proceed with that analysis, it is useful to exploit the largeness of the nondimensional activation energy appearing in the Arrhenius reaction-rate expression and to consider the formal asymptotic limit $N_g \gg 1$. Accordingly, we introduce the Zel'dovich number β defined as

$$\beta = (1 - T_b^{-1}) N_g \gg 1. \quad (45)$$

Then, in the limit $\beta \rightarrow \infty$, it is readily seen that the Arrhenius term is exponentially small unless T is within $O(1/\beta)$ of T_b . All chemical activity is therefore concentrated in an asymptotically thin region located at $\xi = \xi_r > 0$, where the reaction-zone location ξ_r is to be determined. Given our previous assumptions, the purely gaseous region is then comprised of the gas preheat zone $0 < \xi < \xi_r$ in which chemical activity is exponentially small, the thin reaction zone where the gas-phase reactants are consumed, and finally, the burned region $\xi > \xi_r$. Since we anticipate jumps in the derivatives of Y and T at $\xi = \xi_r$ arising from the δ -function-like consumption of reactants and production of heat at that location, we deduce from Eqs. (21) and (23) that these variables themselves are continuous there, taking on the burned values $Y = 0$ and $T = T_b$, respectively. We then conclude from Eq. (36) that u_g is also continuous at $\xi = \xi_r$, where it reaches its burned value u_g^b given by Eq. (37), or equivalently, Eq. (42).

Regarding ξ as the outer variable, analysis of the thin reaction layer requires introducing a stretched, or inner, coordinate, defined in the next section. In the reactionless outer regions, however, we can first integrate Eqs. (20) and (21) for Y , using the results (33) and (36a). Applying the continuity and jump conditions at $\xi = 0$ along with the known value $Y = 0$ at $\xi = \xi_r$, we

deduce that

$$Y(\xi) = \begin{cases} \phi + (Y_c - \phi) \exp\left(\hat{r}\hat{b}Le\xi/\hat{l}\right), & \xi < 0 \\ B_1 + (Y_c - B_1) \exp\left[(1 - \alpha_s + \hat{r}\alpha_s)\hat{b}Le\xi/\hat{l}\right], & 0 < \xi < \xi_r \\ 0, & \xi > \xi_r \end{cases} \quad (46)$$

and

$$\xi_r = \frac{\hat{l}}{\hat{b}}(1 - \alpha_s + \hat{r}\alpha_s)^{-1}Le^{-1} \ln\left(\frac{B_1}{B_1 - Y_c}\right), \quad (47)$$

where

$$B_1 = \frac{(1 - \alpha_s)\beta_c + \phi\hat{r}\alpha_s}{1 - \alpha_s + \hat{r}\alpha_s}. \quad (48)$$

In a similar fashion, we can integrate Eq. (40) subject to $T = T_c$ at $\xi = 0$ and $T = T_b$ at $\xi = \xi_r$ to obtain

$$T(\xi) = \begin{cases} B + (T_c - B) \exp\left[(1 - \alpha_s + \hat{r}\alpha_s)\hat{b}\xi/\hat{l}\right], & 0 < \xi < \xi_r \\ T_b, & \xi > \xi_r \end{cases} \quad (49)$$

and

$$\xi_r = \frac{\hat{l}}{\hat{b}}(1 - \alpha_s + \hat{r}\alpha_s)^{-1} \ln\left(\frac{T_b - B}{T_c - B}\right), \quad (50)$$

where

$$B = T_b - \frac{Q + \gamma_s}{\hat{b}} B_1. \quad (51)$$

Comparison of Eqs. (47) and (50) then implies that Y_c and T_c , which are as yet undetermined, are related according to

$$Y_c = B_1 \left[1 - \left(\frac{T_c - B}{T_b - B} \right)^{Le} \right]. \quad (52)$$

Expressions for Y_c and T_c separately follow from the reaction-zone analysis of the next section, where an expression for the burning-rate eigenvalue Λ_g is determined as well.

Determination of the temperature profile in the reactionless solid-gas region ($\xi < 0$) is more complex in that it is directly coupled, according to Eq. (39) to the gas pressure p_g . However, a scalar equation for p_g alone can be deduced by first solving Eqs. (24) and (34) for T to obtain

$$T = p_g \left(1 - \frac{\kappa}{\alpha_s} \frac{dp_g}{d\xi} \right) \frac{\bar{\phi}}{Y + w(1 - Y)}, \quad \xi < 0, \quad (53)$$

where $Y(\xi)$ is given by Eq. (46). Upon substitution of this result into Eq. (39), we obtain

$$\begin{aligned} & (1 - \alpha_s + \hat{r}\hat{b}\alpha_s) \left[p_g \left(1 - \frac{\kappa}{\alpha_s} \frac{dp_g}{d\xi} \right) \frac{\bar{\phi}}{Y + w(1 - Y)} - 1 \right] \\ & = (1 - \alpha_s + \hat{l}\alpha_s) \frac{d}{d\xi} \left[p_g \left(1 - \frac{\kappa}{\alpha_s} \frac{dp_g}{d\xi} \right) \frac{\bar{\phi}}{Y + w(1 - Y)} \right] + \hat{r}\hat{b}\chi\alpha_s(p_g - 1), \quad \xi < 0, \end{aligned} \quad (54)$$

which is a second-order equation for p_g that is subject to the boundary conditions

$$p_g = p_g^b, \quad \frac{dp_g}{d\xi} = \frac{\alpha_s}{\kappa} \left[1 - \left(\frac{T_c}{p_g^b} \right) \frac{Y_c + w(1 - Y_c)}{\bar{\phi}} \right] \quad \text{at } \xi = 0; \quad (55)$$

$$p_g \rightarrow 1 \quad \text{as } \xi \rightarrow -\infty.$$

Here, the second condition follows from Eqs. (24) and (35) evaluated at $\xi = 0^-$, and the third condition, which is included here only for completeness, has already been applied in the derivation of Eq. (54) through the use of Eq. (39). Consequently, the last of these conditions is identically satisfied by all solutions of Eq. (54), leaving the two surface conditions to uniquely determine the correct one. An asymptotic solution of this nonlinear problem for p_g , from which T and u_g may be calculated according to Eqs. (53) and (34), respectively, can be obtained by exploiting the reasonable limit of weak permeability. However, since the burning-rate eigenvalue can be determined without explicit knowledge of the complete solution in the solid/gas region, we first consider the reaction-zone problem. Solution of the latter will provide an expression for Λ_g , after which we shall complete the above solution in the gas-permeation region $\xi < 0$.

6. Reaction-Zone Solutions and the Burning-Rate Eigenvalue

In order to analyze the chemical boundary layer at ξ_r , we introduce a stretched, or inner, coordinate η as well as a normalized temperature variable θ defined by

$$\eta = \beta(\xi - \xi_r); \quad \theta = \frac{T - 1}{T_b - 1}. \quad (56)$$

Within the reaction zone itself, solutions for the dependent variables and the burning-rate eigenvalue have the asymptotic form

$$\theta \sim 1 + \beta^{-1}\theta_1 + \beta^{-2}\theta_2 + \dots, \quad Y \sim \beta^{-1}y_1 + \beta^{-2}y_2 + \dots, \quad (57)$$

$$\Lambda_g \sim \beta^{n+1} (\Lambda_0 + \beta^{-1}\Lambda_1 + \beta^{-2}\Lambda_2 + \dots),$$

where we note that n is the order of gas-phase reaction and that the corresponding expansions for ρ_g and u_g , if desired, are determined directly from Eqs. (25) and (36b). Substituting these expansions into Eq. (21), using the result (36a), and Eq. (40), we obtain at leading order the coupled equations

$$\frac{\hat{l}}{\hat{b}Le} \frac{d^2 y_1}{d\eta^2} = \Lambda_0 (\rho_g^b)^n y_1^n e^{\theta_1}, \quad (58)$$

$$\frac{d\theta_1}{d\eta} = -\frac{Q + \gamma_s}{\hat{b}(T_b - 1)} Le^{-1} \frac{dy_1}{d\eta}, \quad (59)$$

where we have used the fact that the leading-order term in the expansion of ρ_g is its burned value $\rho_g^b = \bar{\phi} p_g^b / w T_b$. Equations (58) and (59) are to be solved subject to the boundary and matching conditions

$$\theta_1 \rightarrow 0, \quad y_1 \rightarrow 0 \quad \text{as } \eta \rightarrow +\infty, \quad (60)$$

$$\theta_1 \sim \eta (T_b - 1)^{-1} \frac{dT}{d\xi} \Big|_{\xi=\xi_r^-}, \quad y_1 \sim \eta \frac{dY}{d\xi} \Big|_{\xi=\xi_r^-} \quad \text{as } \eta \rightarrow -\infty, \quad (61a)$$

where Y and T here denote the outer solutions obtained in the previous section. Using the outer-solution results (46), (47), (49) and (50), Eqs. (61a) can be rewritten explicitly as

$$\theta_1 \sim \frac{Q + \gamma_s}{\hat{l}(T_b - 1)} [(1 - \alpha_s)\beta_c + \phi \hat{r}\alpha_s] \eta, \quad y_1 \sim \frac{-\hat{b}Le}{\hat{l}} [(1 - \alpha_s)\beta_c + \phi \hat{r}\alpha_s] \eta \quad \text{as } \eta \rightarrow -\infty, \quad (61b)$$

We observe that in this form, the leading-order inner problem is independent of the still undetermined values Y_c and T_c at the material surface, and is thus a closed problem for the leading-order inner variables θ_1 , y_1 and the leading-order eigenvalue coefficient Λ_0 .

The calculation of the eigenvalue now proceeds in much the same fashion as for strictly gaseous flames (*cf.* [11]). We first integrate Eq. (59) subject to the boundary conditions (60), which determines y_1 in terms of θ_1 as

$$y_1 = -\frac{\hat{b}(T_b - 1)}{Q + \gamma_s} Le \theta_1. \quad (62)$$

Substituting this result into Eq. (58) then yields a scalar second-order equation for θ_1 given by

$$\frac{d^2\theta_1}{d\eta^2} = -\frac{\Lambda_0}{\hat{l}} \left(\frac{T_b - 1}{Q + \gamma_s}\right)^{n-1} (\hat{b}Le\rho_g^b)^n (-\theta_1)^n e^{\theta_1}. \quad (63)$$

Next, multiplying each side of Eq. (63) by $d\theta_1/d\eta$ and integrating using the boundary conditions at $\eta = \infty$, we obtain the first integral

$$\begin{aligned} \frac{1}{2} \left(\frac{d\theta_1}{d\eta}\right)^2 &= \frac{\Lambda_0}{\hat{l}} \left(\frac{T_b - 1}{Q + \gamma_s}\right)^{n-1} (\hat{b}Le\rho_g^b)^n \int_{\theta_1}^0 (-\bar{\theta}_1)^n e^{\bar{\theta}_1} d\bar{\theta}_1 \\ &= \frac{\Lambda_0}{\hat{l}} \left(\frac{T_b - 1}{Q + \gamma_s}\right)^{n-1} (\hat{b}Le\rho_g^b)^n \int_0^{-\theta_1} \bar{\theta}_1^n e^{-\bar{\theta}_1} d\bar{\theta}_1. \end{aligned} \quad (64)$$

Finally, evaluating Eq. (64) at $\eta = -\infty$ according to the first of the matching conditions (61b), we obtain an expression for Λ_0 as

$$\Lambda_0 = \left(\frac{Q + \gamma_s}{T_b - 1}\right)^{n+1} \frac{[(1 - \alpha_s)\beta_c + \phi \hat{r}\alpha_s]^2}{2\hat{l}\Gamma(n+1) (\hat{b}Le)^n (\bar{\phi}p_g^b/wT_b)^n}, \quad (65)$$

where $\Gamma(n+1) = n!$ for nonnegative integer reaction orders. Limiting expressions are clearly obtained when $\phi \rightarrow 0$ (no reactants deep within the porous solid) and $\alpha_s \rightarrow 0$ (zero porosity). In the latter case, the expression for Λ_0 essentially collapses to previous results that have been obtained for nonporous propellants (*cf.* [8]). It is also of interest to note that in the limit $\beta_c \rightarrow 0$, reflecting the complete conversion of the solid to gaseous products via surface pyrolysis, the presence of reactants within the unburned solid ($\phi > 0$) becomes rate-controlling.

The dimensional formula for the leading-order approximation of the propagation speed \tilde{U} is readily derived from the above expression for Λ_0 , the relationship of Λ_0 to Λ_g given by Eq. (57),

and the definition of Λ_g and the other nondimensional parameters given in Eqs. (17) and (45). In particular, we obtain

$$\tilde{U}^2 \sim \frac{\tilde{\lambda}_s \tilde{A}_g (\tilde{\rho}_g^u)^n}{\beta^{n+1} \Lambda_0 \tilde{\rho}_s^2 \tilde{c}_s} e^{-N_g} = \frac{2\hat{r}\hat{l} T_b^{n+2} (\hat{b} Le \bar{\phi} p_g^b / w)^n \Gamma(n+1)}{[N_g^u (Q + \gamma_s)]^{n+1} [(1 - \alpha_s)\beta_c + \phi\hat{r}\alpha_s]^2} (\tilde{\rho}_g^u)^{n-1} \tilde{a} \tilde{A}_g e^{-N_g^u / T_b}, \quad (66)$$

where we have introduced the additional definitions $N_g^u = \tilde{E}_g / \tilde{R}^\circ \tilde{T}_u = N_g T_b$ and $\tilde{a} = \tilde{\lambda}_s / \tilde{\rho}_s \tilde{c}_s$. We observe that \tilde{U} depends implicitly on the overpressure through the linear dependence of T_b on $p_g^b - 1$ expressed in Eq. (41), as well as any pressure dependence that may be ascribed to the rate constant \tilde{A}_g . As in a previous study [3], this overpressure dependence is conveniently studied by introducing the normalized propagation speed $U^* = \tilde{U}(p_g^b) / \tilde{U}(1)$, where the argument denotes the value of p_g^b . Consequently, $U^* = U_n [\tilde{A}_g(p_g^b) / \tilde{A}(1)]^{1/2}$, where, having factored out the rate-constant influence, U_n is given by

$$U_n = (p_g^b)^{n/2} \left[\frac{T_b(p_g^b)}{T_b(1)} \right]^{(n+2)/2} \exp \left\{ \frac{N_g^u}{2} \left[\frac{1}{T_b(1)} - \frac{1}{T_b(p_g^b)} \right] \right\}. \quad (67)$$

Since N_g^u , which is a nondimensional activation energy defined with respect to the *unburned* temperature \tilde{T}_u , is typically quite large, it is clear that the pressure sensitivity of the burning rate is predominantly exponential for modest values of overpressure. However, as p_g^b increases, T_b also increases; consequently, this exponential sensitivity is gradually diminished as the last factor in Eq. (67) varies less and the algebraic influence of the two prefactors begins to dominate.

These results are shown in Figure 4 for $n = 1$ and several values of porosity. Qualitatively similar results were obtained using an alternative model in which the present surface and gas-phase reactions are replaced with a melting condition followed by a distributed liquid-to-gas reaction [3]. Indeed, the main difference lies in the form of the algebraic prefactors that reflect the differences associated with the specific type of distributed reaction in each of the two models. In the present case, we expect the reaction order n to lie in the range $1 \leq n < 2$, corresponding to the behavior $U_n \sim (p_g^b)^{n+1}$ (for $\alpha_s > 0$) in the limit $p_g^b \gg 1$. We remark that these two-phase-flow effects all vanish in the nonporous limit $\alpha_s \rightarrow 0$, since there is then no gas permeation and hence no convection-enhanced acceleration in the burning rate with increasing overpressure. This result is indicated by the $\alpha_s = 0$ curve in Figure 4, which depicts only a gradual increase in the propagation speed with gas pressure, namely $U_n \sim (p_g^b)^{1/2}$, that is typical of “conductive” burning (*cf.* [1],[2]).

We observe from Figure 4 that there is a more rapid increase in the burning rate with increasing overpressure for larger porosities. Indeed, defining a new normalized propagation speed $U^{**} = \tilde{U}(\alpha_s) / \tilde{U}(0)$, where the argument now denotes the value of α_s , we calculate

$$U^{**} = \frac{\beta_c}{(1 - \alpha_s)\beta_c + \phi\hat{r}\alpha_s} \left[\frac{T_b(\alpha_s)}{T_b(0)} \right]^{(n+2)/2} \exp \left\{ \frac{N_g^u}{2} \left[\frac{1}{T_b(0)} - \frac{1}{T_b(\alpha_s)} \right] \right\}. \quad (68)$$

Plots of U^{**} as a function of α_s for several values of p_g^b and ϕ are exhibited in Figure 5. As indicated by Eq. (68) and reflecting the strong influence of two-phase-flow effects, there is, for any given overpressure, a predominantly exponential increase in the burning rate with respect to positive variations in α_s . Consistent with its effect on T_b , a larger fraction ϕ of reactants deep within the porous solid also results in a faster propagation speed.

Having determined an approximate expression for Λ_g , and hence \tilde{U} , an expression for the surface temperature T_c can be determined from the result (32) for Λ_s and either its definition in Eq. (17) or from the relationship (18) between Λ_s and Λ_g . In particular, using the definition $N_s^u = \tilde{E}_s/\tilde{R}^o\tilde{T}_u = N_s T_c$ in either expression for Λ_s , one can solve for T_c to obtain

$$T_c = \frac{N_s^u}{\ln [\tilde{A}_s/(\tilde{\rho}_s\tilde{U})]} = 2N_s^u \ln^{-1} \left\{ \frac{[N_g^u(Q + \gamma_s)]^{n+1} [(1 - \alpha_s)\beta_w + \phi\hat{r}\alpha_s]^2 e^{N_g^u/T_b}}{2\hat{r}\hat{l}T_b^{n+2}(\hat{b}Le\bar{\phi}p_g^b/w)^n \Gamma(n+1)} \cdot \frac{\tilde{A}_s^2/\tilde{A}_g}{\tilde{a}\tilde{\rho}_s^2(\tilde{\rho}_g^u)^{n-1}} \right\}, \quad (69)$$

which in turn determines ξ_r and Y_c according to Eqs. (50) and (52), respectively.

Several trends and limiting cases, which imply certain restrictions on the admissible parameter regime required for consistency with the present solution, are immediately evident. First, from Eq. (69), the fact that T_c must exceed the unburned temperature of unity implies that the largest possible range for \tilde{U} is $(\tilde{A}_s/\tilde{\rho}_s)e^{-N_s^u} < \tilde{U} < \tilde{A}_s/\tilde{\rho}_s$, where the last inequality follows from the physical restriction of T_c to positive values. Within this range, increases in T_b will increase \tilde{U} according to Eq. (66), and thus increase T_c according to Eq. (69). Similarly, decreasing the fraction β_c of material that first sublimates enhances the propagation speed while leaving the burned temperature T_b , which is independent of this parameter, unaffected. Decreasing the unburned reactant mass fraction ϕ , on the other hand, reduces T_b and hence tends to diminish T_c .

As indicated in the Introduction, it is readily anticipated that when the overpressure increases from zero, the reversal in the direction of gas flow causes the location $\xi = \xi_r$ of the gaseous reaction zone to decrease, eventually approaching the material surface and marking the end of the parameter regime for which the present analysis is valid. That is, as ξ_r approaches zero, the strictly gaseous preheat region disappears and a new analysis to describe a gas flame in the vicinity of the material surface is required. The location ξ_r , which is now determined by Eqs. (50) and (69), may first be expressed in terms of T_c and T_b using the definitions (48) and (51) as

$$\xi_r = -\frac{\hat{l}}{\hat{b}(1 - \alpha_s + \hat{r}\alpha_s)} \ln \left\{ 1 - (T_b - T_c) \frac{\hat{b}(1 - \alpha_s + \hat{r}\alpha_s)}{(Q + \gamma_s)[(1 - \alpha_s)\beta_c + \phi\hat{r}\alpha_s]} \right\}. \quad (70)$$

Thus, $\xi_r \rightarrow 0$ as $T_c \rightarrow T_b$, where T_c and T_b are given by Eqs. (41) and (69) in terms of the various parameters. This result is illustrated in Figures 6a and 6b, where both T_c and T_b are plotted against overpressure for characteristic values of the remaining parameters. Critical values of overpressure where these curves intersect thus denote the onset of the aforementioned intrusive flame regime. We observe from a comparison of Figures 6a and 6b that larger values of the

surface activation-energy parameter N_s^u , which correspond to slower rates of surface sublimation and pyrolysis, lead to smaller critical values of overpressure. Conversely, larger ratios of the surface reaction rate and/or smaller values of the gaseous reaction rate, as represented by the parameter ratio $M = (\tilde{A}_s/\tilde{A}_g^{1/2})/[\tilde{a}\tilde{\rho}_s^2(\tilde{\rho}_g^u)^{n-1}]^{1/2}$, lead to larger critical values of p_g^b , or none at all. The latter thus implies the existence of a gaseous preheat region for all overpressures. In the opposite limit that $T_b - T_c \rightarrow (Q + \gamma_s)[(1 - \alpha_s)\beta_c + \phi\hat{r}\alpha_s]/[\hat{b}(1 - \alpha_s + \hat{r}\alpha_s)]$, corresponding to a nonzero critical difference between T_b and T_c , the reaction-zone location ξ_r approaches infinity. Thus, from the expression (41) for T_b , this occurs in the limit $T_c \rightarrow T_c^*$, where T_c^* is given by

$$T_c^* = \frac{(1 - \alpha_s)[Q + 1 - \beta_c(Q + \gamma_s)] + \hat{r}\hat{b}\alpha_s[\chi(p_g^b - 1) + 1]}{\hat{b}(1 - \alpha_s + \hat{r}\alpha_s)}. \quad (71)$$

In the present parameter regime, T_c therefore lies in the range $T_c^* < T_c < T_b$, corresponding to the range of propagation speeds $(\tilde{A}_s/\tilde{\rho}_s)e^{-N_s^u/T_c^*} < \tilde{U} < (\tilde{A}_s/\tilde{\rho}_s)e^{-N_s^u/T_b}$ and the flame standoff distances $\infty > \xi_r > 0$. This range of propagation speeds for the present burning regime is thus narrower than that given in the general case below Eq. (69).

As a final note, the expression for the surface temperature T_c given by Eq. (69) allows one to calculate $u_g^\pm = u_g|_{\xi=0^\pm}$ according to Eqs. (29) and (35). These results are illustrated in Figure 7, which emphasizes the discontinuity in gas velocity at the material surface and demonstrates that the flow of gas is directed into the porous solid (*i.e.*, $u_g^- < 0$) for relatively modest values of the overpressure. At somewhat larger values of overpressure, u_g^+ , which is larger than u_g^- due to the production of gas at the material surface, becomes negative as well. Finally, for sufficiently large values of p_g^b , even the burned-gas velocity u_g^b becomes negative, as was shown in Figure 3.

7. Conclusions

The present work reflects a further refinement in describing the effects of overpressure and the consequent burned-gas permeation on the quasi-steady propagation of deflagrations in porous energetic materials under confinement. In particular, the replacement of the surface melt layer, which is commonly observed in unconfined nitramine deflagration, with the sublimation, pyrolysis and gaseous reactions used in the present model is more physically realistic at larger overpressures. Consequently, additional effects associated with the presence of unburned reactants in the solid/gas region and the resulting differences in the structure of the combustion wave lead to corresponding modifications in the expression for the burning rate.

The functional form of the normalized burning rate once again reflects the change in the pressure sensitivity of the propagation speed with increasing overpressure. At lower overpressures, the exponential factor in those expressions dominates owing to the large activation energy of the gas-phase reaction. However, at larger overpressures, this factor becomes less dominant and the algebraic dependence on the burned-gas pressure reflected in the prefactors then tend to determine

the burning-rate pressure sensitivity. This results in a transition from a less pressure-sensitive to a more pressure sensitive burning-rate response as the overpressure increases, where these two regimes have historically been interpreted as the “conductive” and “convective” branches of the overall response. We note that the exponential factor is similar to that obtained when the model is based on the presence of a surface melt layer, but that the algebraic prefactors are quite different and reflect the significant differences between that model and the present one. In addition, the mass fraction ϕ of gaseous reactants deep within the porous solid, which is absent in the earlier formulation, affects the value of the burned temperature T_b and is thus implicitly present in both the exponential and algebraic factors in the burning-rate expression.

The generally accepted terminology regarding the aforementioned branches of the burning-rate response reflects the assumed dominance of either conduction or convection, respectively, in determining the propagation speed. However, analyses such as that presented here make it clear that both effects are always present to some extent throughout the transition from “conductive” to “convective” burning. In particular, the gaseous reaction region remains diffusion-controlled while convection is responsible for the burned-gas permeation into the porous solid and the consequent preheating of the unburned material. An increase in overpressure serves to primarily increase the importance of the latter, which in turn results in higher combustion temperatures and hence faster reaction rates.

The present model also admits at least two distinctive wave structures. In the analysis presented here, it was assumed that there exists a gaseous preheat zone that separates the attached gas flame from the material surface, and conditions for this to be true were derived. In addition, however, there exists a regime in which the gas flame lies in the vicinity of this surface. In that case, the preheat zone lies wholly within the solid/gas region, and the material surface then lies within the gas-phase reaction zone such that the sublimation, pyrolysis and gas-phase reactions all occur in a single merged-flame region. An analysis of this scenario, which generally can occur only at sufficiently large overpressures, will be considered in a future study.

Appendix. The Gas-Permeation Region

Although the profiles of gas pressure, temperature and gas velocity in the solid/gas region were not required in order to determine the leading-order expression for the burning-rate eigenvalue and other quantities of interest described above, it is nonetheless of interest to consider this two-phase-flow region further. In particular, it is the pressure-driven gas permeation into the porous material that is responsible for the acceleration in the burning rate with increasing overpressure, and it is therefore revealing to describe this process in greater detail. We thus consider in some detail the solution of the problem (54) and (55) for p_g since, according to Eqs. (24) and (53), both the gas velocity and temperature can be calculated once the gas pressure is known.

For convenience, we first introduce the overpressure variable $p = p_g - 1$ and the function $f(\xi) = \bar{\phi}/[Y + w(1 - Y)]$, where $Y(\xi)$ for $\xi < 0$ was given by Eqs. (46) and (52). In terms of these quantities, Eqs. (54) and (55) are expressed as

$$\begin{aligned} & (1 - \alpha_s + \hat{r}\hat{b}\alpha_s) \left[(p + 1)f(\xi) - \frac{\kappa}{\alpha_s}(p + 1)f(\xi)\frac{dp}{d\xi} - 1 \right] \\ & = (1 - \alpha_s + \hat{l}\alpha_s)\frac{d}{d\xi} \left[(p + 1)f(\xi) - \frac{\kappa}{\alpha_s}(p + 1)f(\xi)\frac{dp}{d\xi} \right] + \hat{r}\hat{b}\chi\alpha_s p, \quad \xi < 0, \end{aligned} \quad (\text{A.1})$$

subject to

$$\begin{aligned} p = p_g^b - 1 = p_b, \quad \frac{dp}{d\xi} = \frac{\alpha_s}{\kappa} \left[1 - \left(\frac{T_c}{p_b + 1} \right) \frac{1}{f(0)} \right] \quad \text{at } \xi = 0; \\ p \rightarrow 0 \quad \text{as } \xi \rightarrow -\infty, \end{aligned} \quad (\text{A.2})$$

where $f(0) = \bar{\phi}/[Y_c + w(1 - Y_c)]$. Exploiting the realistic limit of weak permeability ($\kappa \ll 1$), we anticipate from the second of Eqs. (A.2) that there exists a boundary layer with respect to the gas-pressure variable p , and hence the gas velocity u_g , adjacent to the material surface $\xi = 0$, provided p itself is regarded as an $O(1)$ quantity. The analysis of this boundary layer then proceeds in a similar fashion to that given previously in connection with the alternative model described above ([3],[12]).

We formalize the analysis by introducing a bookkeeping parameter $\epsilon \ll 1$ and defining the scaled permeability $\kappa = \kappa^*\epsilon$. All remaining quantities are, for the moment, regarded as $O(1)$, although additional simplifications do occur if \hat{r} and/or \hat{l} are also regarded as small. In this context we note there is no connection between ϵ and the inverse Zel'dovich number β^{-1} , although it is reasonable to assume that $\beta^{-1} \ll \epsilon \ll 1$. In that case, the thickness of the gas-permeation layer is small, but much thicker than the gaseous reaction zone. Solutions to Eqs. (A.1) and (A.2) are then sought as matched asymptotic expansions of the form

$$p^{(i)} \sim p_0(\hat{\eta}) + \epsilon p_1(\hat{\eta}) + \dots, \quad p^{(o)} \sim q_0(\xi) + \epsilon q_1(\xi) + \dots, \quad (\text{A.3})$$

where $p^{(i)}$ denotes the inner, or boundary-layer, solution as a function of the stretched inner coordinate $\hat{\eta} = \xi/\epsilon$, and $p^{(o)}$ represents the outer solution as a function of the outer coordinate ξ . Substituting the first of these expansions into Eqs. (A.1) and (A.2) and collecting the lowest-order terms, the leading-order inner problem for the coefficient p_0 in the inner expansion is obtained as

$$\frac{d}{d\hat{\eta}} \left[p_0 - \frac{\kappa^*}{\alpha_s}(p_0 + 1)\frac{dp_0}{d\hat{\eta}} \right] = 0, \quad (\text{A.4})$$

$$p_0 = p_b, \quad \frac{dp_0}{d\hat{\eta}} = \frac{\alpha_s}{\kappa^*} \left[1 - \left(\frac{T_c}{p_b + 1} \right) \frac{1}{f(0)} \right] \quad \text{at } \hat{\eta} = 0. \quad (\text{A.5})$$

Integrating Eq. (A.4) twice and applying the boundary conditions (A.5), we obtain an implicit boundary-layer solution for the leading-order overpressure p_0 as

$$\frac{\alpha_s}{\kappa^*}\hat{\eta} = p_0 - p_b + \frac{T_c}{f(0)} \ln \left[\frac{p_0 + 1 - T_c/f(0)}{p_b + 1 - T_c/f(0)} \right]. \quad (\text{A.6})$$

As expected, the inner solution (A.6) does not satisfy the last of Eqs. (A.2) since $p_0 \rightarrow T_c/f(0) - 1 > 0$ as $\hat{\eta} \rightarrow -\infty$. We thus consider the outer problem for $p^{(o)}$ on the scale of the outer coordinate ξ . In particular, the leading-order outer problem for the coefficient q_0 in the outer expansion is given by

$$(1 - \alpha_s + \hat{r}\hat{b}\alpha_s) [(q_0 + 1)f(\xi) - 1] = (1 - \alpha_s + \hat{l}\alpha_s) \frac{d}{d\xi} [(q_0 + 1)f(\xi)] + \hat{r}\hat{b}\chi\alpha_s q_0. \quad (\text{A.7})$$

While an explicit formal solution of this linear, first-order, ordinary differential equation can be written down in an integral form, the form of $f(\xi)$, which in turn depends on $Y(\xi)$, renders that form of the solution intractable. We thus consider the reasonable limits in which either \hat{r} and/or \hat{l} are small, which was the approach taken in previous work ([3],[12]).

Considering first the regime in which $\hat{r} \sim O(\epsilon)$ while \hat{l} remains an $O(1)$ quantity, we define the scaled gas-to-solid density-ratio parameter $\hat{r}^* = \hat{r}/\epsilon$. In this limit, the mass fraction Y of gas reactants varies, according to Eq. (46), on a much larger $O(1/\epsilon)$ spatial scale. Consequently, $Y = Y_c$ to leading order within the $O(1)$ distances from the material surface of interest here. Hence, $f(\xi) \sim f(0)$ for $\xi \sim O(1)$, and Eq. (A.7) reduces to

$$(1 - \alpha_s)[q_0 + 1 - 1/f(0)] = (1 - \alpha_s + \hat{l}\alpha_s) \frac{dq_0}{d\xi}, \quad (\text{A.8})$$

the solution to which is given explicitly as $q_0 = 1/f(0) - 1 + c_1 \exp[(1 - \alpha_s)\xi/(1 - \alpha_s + \hat{l}\alpha_s)]$. Matching with the inner solution (A.6), which is unchanged, as $\xi \rightarrow 0$ yields the integration constant $c_1 = (T_c - 1)/f(0)$. Thus, the solution of Eq. (A.8) for q_0 in the outer region is given by

$$q_0(\xi) = \frac{1 - f(0)}{f(0)} + \frac{T_c - 1}{f(0)} \exp\left[\frac{1 - \alpha_s}{1 - \alpha_s + \hat{l}\alpha_s} \xi\right]. \quad (\text{A.9})$$

However, since $q_0 \rightarrow 1/f(0) - 1 \neq 0$ as $\xi \rightarrow -\infty$, the last boundary condition in Eq. (A.2) is still unsatisfied except when the molecular-weight ratio $w = 1$ (in which case $f \equiv 1$). Satisfaction of this condition for arbitrary w thus requires construction of the solution for the overpressure p in the far-outer region $\xi \sim O(1/\epsilon)$ over which $Y(\xi)$ varies from its surface value Y_c to its value ϕ deep within the porous solid. We therefore define the far-outer coordinate $\zeta = \epsilon\xi$ and seek the far-outer solution for overpressure in the form of the expansion $p^{(fo)} \sim r_0(\zeta) + \epsilon r_1(\zeta) + \dots$. From Eq. (A.1), we find that r_0 satisfies the algebraic equation $(1 - \alpha_s)[(r_0 + 1)f(\zeta) - 1] = 0$, or

$$r_0(\zeta) = \frac{1 - f(\zeta)}{f(\zeta)}, \quad (\text{A.10})$$

where f is now written as a function of ζ by virtue of the fact that in the present regime, we have, according to Eq. (46), $Y = Y(\zeta) = \phi + (Y_c - \phi)e^{\hat{r}^*\hat{b}Le\zeta/\hat{l}}$. We note that since $f \rightarrow 1$ as $\zeta \rightarrow -\infty$, the leading-order coefficient $r_0 \rightarrow 0$ in that limit, which thus satisfies the last boundary condition

in Eq. (A.2). In addition, $r_0 \rightarrow 1/f(0) - 1$ as $\zeta \rightarrow 0$, so that the far-outer solution (A.10) properly matches with the outer solution (A.9).

A leading-order, uniformly-valid, composite solution for the parameter regime just described is readily obtained from Eqs. (A.6), (A.9) and (A.10) as

$$\begin{aligned} p &\sim p^{(i)} + p^{(o)} + p^{(fo)} - \lim_{\xi \rightarrow 0} p^{(o)} - \lim_{\xi \rightarrow -\infty} p^{(o)} \\ &= p_0(\xi/\epsilon) + [(T_c - 1)/f(0)] \exp \left[\frac{1 - \alpha_s}{1 - \alpha_s + \hat{l}\alpha_s} \xi \right] + \frac{1 - f(\epsilon\xi)}{f(\epsilon\xi)} - \frac{T_c - f(0)}{f(0)}, \end{aligned} \quad (\text{A.11})$$

where the implicit inner solution $p_0(\hat{\eta})$ has been expressed functionally in terms of the outer variable ξ , and similarly for $f(\zeta)$. The inner, outer, far-outer and composite solutions for the overpressure in the solid/gas region are exhibited in Figures 8a–c. Figure 8a is a typical case, but it is of interest to note, as illustrated in Figures 8b and 8c, that the pressure profile need not be monotonic. In particular, we note that the quantity $1/f(0) - 1 = (\phi - Y_c)(w - 1)/[\phi + w(1 - \phi)]$, which corresponds to both the outer limit of the far-outer solution r_0 and the far-outer limit of the outer solution q_0 , can in principle take on negative values in the range $1/f(0) > -1$, where the lower limit follows from the fact that $f(0) > 0$. This results in a negative overpressure (*i.e.*, a value of pressure that is greater than zero but less than unity) over the far-outer portion of the gas-permeation region, as shown in Figure 8c. Because the overall molecular weight of the reactant species usually exceeds that of the product, it is reasonable to assume $w > 1$ and thus this situation occurs for $\phi < Y_c$, which implies a sufficient degree of reactant production via sublimation (as opposed to direct pyrolysis) at the material surface. In this case, Y is nonmonotonic as well and thus the heavier reactants produced at the surface tend to diffuse in both the positive direction (toward the reactant-consuming gaseous flame) and into the porous solid itself.

The present boundary-layer construction of the gas-permeation region is primarily valid for the parameter range $p_b > T_c/f(0) - 1$, in which case the gradient at the material surface is, according to Eq. (A.2), large and negative as illustrated in Figures 8a and 8b. In this range of overpressures, both the pressure and gas velocity, which is directed into the porous solid, have a boundary-layer character, indicating that the weak permeability of the porous material permits only a relatively shallow permeation of the gas for $O(1)$ overpressures. We note that a deeper, $O(1)$ penetration is achieved for larger-magnitude overpressures [3], and in the opposite limit that $p_b \downarrow T_c/f(0) - 1$, the pressure gradient ceases to be large and the present boundary-layer analysis breaks down. Indeed, for overpressures below this limit, the pressure gradient at the material surface is negative, indicating a flow of gas out of the solid as in the case of an unconfined deflagration [6]. For $p_b < T_c/f(0) - 1$, the boundary-layer construction again becomes valid provided $T_c/f(0) - (p_b + 1) \sim O(1)$, as shown in Figure 8d. Then, in contrast to the previous situation in which the gas flow was slowed as it was driven into the solid by a strong overpressure $p_b > T_c/f(0) - 1$, the weak permeability of the porous material now inhibits the gas as it flows *out*

of the solid, corresponding to a negative pressure gradient according to Darcy's law. The resulting local pressure maximum that occurs near the material surface, which implies a corresponding turning point in the Darcy flow velocity, arises from the preheating of the gas by thermal diffusion. Indeed, in this regime of very modest overpressures, this effect is more significant than overpressure-driven convection, thereby allowing the pressure in the solid/gas region to exceed p_b .

Based on the asymptotic construction for the overpressure $p(\xi)$ described above, a corresponding uniform approximation for the gas velocity $u_g(\xi)$ may be obtained either by calculating the expression for u_g in each region and constructing a composite solution, or by simply substituting the uniformly valid result (A.11) into the expression for Darcy's law given by Eq. (24). Based on the latter approach, the velocity profiles corresponding to the three cases exhibited in Figures 8a, 8b-c and 8d are shown in Figure 9, where a zero, or turning point, in the flow velocity corresponds to either a local minimum or maximum in the pressure profile. This is most clearly seen in the velocity profile corresponding to Figure 8d, where u_g is positive near the propellant surface where the pressure gradient is negative, but becomes negative as ξ decreases and p passes through its local maximum.

Another reasonable parameter regime is one in which both \hat{r} and \hat{l} are small; that is, $\hat{r} = \hat{r}^* \epsilon$ and $\hat{l} = \hat{l}^* \epsilon$. This regime was considered previously in the context of the melting model referred to above ([3],[12]), and is essentially a simplification of the preceding results. In particular, the leading-order inner problem and solution is again given by Eqs. (A.4) – (A.6), while the outer problem is somewhat different because now Y , and hence f , vary on the $O(1)$ outer scale ξ . Thus, in place of Eq. (A.8), we obtain from Eq. (A.7) the equation for q_0 as

$$(q_0 + 1)f(\xi) - 1 = \frac{d}{d\xi} [(q_0 + 1)f(\xi)]. \quad (\text{A.12})$$

Solving Eq. (A.12) and matching with the inner solution, we obtain

$$q_0(\xi) = \frac{1}{f(\xi)} [1 + (T_c - 1)e^\xi] - 1, \quad (\text{A.13})$$

which satisfies the boundary condition $q_0 \rightarrow 0$ as $\xi \rightarrow -\infty$. Thus, because Y varies from ϕ to its surface value Y_c on the ξ scale, the overpressure also varies from 0 to p_b on this scale and thus there is no need to introduce a far-outer region in this case. As a result, a leading-order composite solution in this parameter regime is obtained from Eqs. (A.6) and (A.13) as

$$\begin{aligned} p &\sim p^{(i)} + p^{(o)} - \lim_{\xi \rightarrow 0} p^{(o)} \\ &= p_0(\xi/\epsilon) + \frac{1}{f(\xi)} [1 + (T_c - 1)e^\xi] - \frac{T_c}{f(0)}, \end{aligned} \quad (\text{A.14})$$

Finally, we briefly consider the case in which the gas-to-solid thermal conductivity ratio is small (*i.e.*, $\hat{l} = \hat{l}^* \epsilon$) while \hat{r} remains $O(1)$. While not as common as the two preceding regimes, it

is nonetheless of interest by virtue of the different structure that emerges. In particular, according to Eq. (46), Y (and hence f) now vary on the $O(\epsilon)$, or $\hat{\eta}$, spatial scale and thus there is now a boundary layer with respect to Y as well as p . As a result, $Y \sim \phi$ and $f(\xi) \sim 1$ in the outer region, while in the inner zone, Eq. (A.4) is replaced by

$$\frac{d}{d\hat{\eta}} \left[(p_0 + 1)f(\hat{\eta}) - \frac{\kappa^*}{\alpha_s}(p_0 + 1)f(\hat{\eta}) \frac{dp_0}{d\hat{\eta}} \right] = 0, \quad (\text{A.15})$$

where $f(\hat{\eta}) = \bar{\phi} / \{Y(\hat{\eta}) + w[1 - Y(\hat{\eta})]\}$ is now properly written as a function of $\hat{\eta}$. Integrating Eq. (A.15) once using the boundary condition (A.5) yields a first-order equation for p_0 given by

$$\frac{dp_0}{d\hat{\eta}} = \frac{\alpha_s}{\kappa^*} \left[1 - \frac{T_c}{(p_0 + 1)f(\hat{\eta})} \right]. \quad (\text{A.16})$$

While this can be solved formally, the resulting integral expression for p_0 cannot be evaluated in closed form. On the other hand, the outer problem is readily tractable since, in place of Eq. (A.7), the equation for q_0 is given by

$$\left[1 - \alpha_s + \hat{r}\hat{b}\alpha_s(1 - \chi) \right] q_0 = (1 - \alpha_s) \frac{dq_0}{d\xi}. \quad (\text{A.17})$$

The solution for q_0 is thus given by

$$q_0 = c_1 \exp \left[\frac{1 - \alpha_s + \hat{r}\hat{b}\alpha_s(1 - \chi)}{(1 - \alpha_s)} \xi \right], \quad (\text{A.18})$$

where the integration constant $c_1 = \lim_{\hat{\eta} \rightarrow -\infty} p_0(\hat{\eta})$ is obtained from matching with the inner solution. We observe that $q_0 \rightarrow 0$ as $\xi \rightarrow -\infty$, and thus there is again no need to introduce a far-outer region to satisfy the last boundary condition in Eq. (A.2).

Acknowledgment

This work was supported by the United States Department of Energy under Contract DE-AC04-94AL85000. Useful discussions with Prof. Forman Williams are gratefully acknowledged.

References

- [1] Boggs, T. L., “The Thermal Behavior of Cyclotrimethylenetrinitramine (RDX) and Cyclotetramethylenetetranitramine (HMX),” in *Fundamentals of Solid-Propellant Combustion* (K. K. Kuo and M. Summerfield, Eds.), *Progress in Astronautics and Aeronautics – Vol. 90*, AIAA, New York, 1984, pp. 121–175.
- [2] Asay, B. W., Son, S. F., and Bdzil, J. B., “The Role of Gas Permeation in Convective Burning,” *International Journal of Multiphase Flow* 22:923–952 (1996).
- [3] Margolis, S. B., “Influence of Pressure-Driven Gas Permeation on the Quasi-Steady Burning of Porous Energetic Materials,” *Combustion Theory and Modelling* 2:95–113 (1998).
- [4] Margolis, S. B., Armstrong, R. C. “Two Asymptotic Models for Solid Propellant Combustion,” *Combustion Science and Technology* 47:1–38 (1986).
- [5] Margolis, S. B., Williams, F. A. and Armstrong, R. C. “Influences of Two-Phase Flow in the Deflagration of Homogeneous Solids,” *Combustion and Flame* 67:249–258 (1987).
- [6] Margolis, S. B., Williams, F. A. “Effects of Two-Phase Flow on the Deflagration of Porous Energetic Materials,” *Journal of Propulsion and Power* 11:759–768 (1995).
- [7] Denison, M. R., Baum, E. “A Simplified Model of Unstable Burning in Solid Propellants,” *ARS Journal* 31:1112-1122 (1961).
- [8] Margolis, S. B., Williams, F. A. “Diffusional/Thermal Coupling and Intrinsic Instability of Solid Propellant Combustion,” *Combustion Science and Technology* 59:27–84 (1988).
- [9] Margolis, S. B., Williams, F. A. “Diffusional/Thermal Instability of a Solid Propellant Flame,” *SIAM Journal* 49:1390-1420 (1989).
- [10] Baer, M. R., and Shepherd, J. E., *A Thin Flame Model for Reactive Flow in Porous Materials*, Sandia National Laboratories Report No. SAND83–2576, 1984.
- [11] Williams, F. A., *Combustion Theory*, Benjamin-Cummings, 1985.
- [12] Telengator, A. M., Margolis, S. B., and Williams, F. A., “Stability of Quasi-Steady Deflagrations in Confined Porous Energetic Materials,” *Combustion Science and Technology* 160:259–316 (2000).

Figure Captions

1. Combustion-wave structure corresponding to the present model of deflagrations in confined porous materials.
- 2a,b. The burned temperature T_b as a function of the overpressure p_b for various values of the reactant mass-fraction parameter ϕ and two different values of porosity α_s given by (a) $\alpha_s = 0.1$ and (b) $\alpha_s = 0.3$. The remaining parameters in the expression for T_b were assigned the values $\chi = 0.3$, $\hat{r} = 0.08$, $\hat{b} = 1.0$, $\gamma_s = 1.0$ and $Q = 8.0$.
- 3a,b. The burned gas velocity u_g^b as a function of the overpressure p_b for various values of the reactant mass-fraction parameter ϕ and two different molecular-weight ratios w given by (a) $w = 0.5$ and (b) $w = 2.0$. The remaining parameters in the expression for u_g^b were assigned the values $\alpha_s = 0.3$, $\chi = 0.3$, $\hat{r} = 0.08$, $\hat{b} = 1.0$, $\gamma_s = 1.0$ and $Q = 8.0$.
4. Normalized propagation speed U_n as a function of the overpressure p_b for several values of the porosity α_s . The remaining parameters in the expression for U_n were assigned the values $N_g^u = 95.0$, $\phi = 0$, $\chi = 0.3$, $\hat{r} = 0.08$, $\hat{b} = 1.0$, $\gamma_s = 1.0$ and $Q = 8.0$.
5. Normalized propagation speed U^{**} as a function of the porosity α_s for several values of the reactant mass-fraction parameter ϕ and the overpressure p_b . The remaining parameters in the expression for U^{**} were assigned the values $N_g^u = 95.0$, $\beta_c = 0.75$, $\phi = 1.0$, $\chi = 0.3$, $\hat{r} = 0.08$, $\hat{b} = 1.0$, $\gamma_s = 1.0$ and $Q = 8.0$.
- 6a,b. The material-surface temperature T_c as a function of the overpressure p_b for various values of the rate-ratio parameter M and characteristic values of the remaining parameters. Also shown is the burned temperature T_b , where the gas-flame standoff distance ξ_r approaches zero as $T_c \rightarrow T_b$. The curves in (a) were drawn for $N_s^u = 80.0$, while those in (b) correspond to $N_s^u = 85.0$. In both figures, the remaining parameters were assigned the values $N_g^u = 95.0$, $\alpha_s = 0.3$, $\phi = 1.0$, $\chi = 0.3$, $\hat{r} = 0.08$, $\hat{b} = 1.0$, $\gamma_s = 1.0$ and $Q = 8.0$.
7. Gas velocities u_g^\pm on either side of the material surface as a function of the overpressure p_b for several values of ϕ . The remaining parameters were assigned the values $M = 7.2$, $N_g^u = 95.0$, $N_s^u = 85.0$, $\alpha_s = 0.3$, $Le = 1.0$, $\beta_c = 0.75$, $\phi = 1.0$, $\chi = 0.3$, $w = 0.5$, $\hat{r} = 0.08$, $\hat{b} = 1.0$, $\gamma_s = 1.0$ and $Q = 8.0$.
- 8a-d. Triple-deck structure of the overpressure variable $p = p_g - 1$ in the solid/gas region $\xi < 0$. Shown are the inner, outer, far-outer and composite asymptotic solutions in the weak-permeability limit $\kappa \sim O(\epsilon) \ll 1$. (a) Example of a monotonic pressure profile for sufficiently large overpressures $p_b > T_c/f(0) - 1$ corresponding to a positive pressure gradient at the material surface ($p_b = 25.0$, $\kappa^* = 0.2$, $\beta_c = 0.95$, $\alpha_s = 0.3$, $\phi = 1.0$, $\hat{r} = 0.05$ and $w = 2.0$). (b) A nonmonotonic profile for burned overpressures $p_b > T_c/f(0) - 1$ ($p_b = 7.0$, $\kappa^* = 0.2$,

$\beta_c = 0.95$, $\alpha_s = 0.1$, $\phi = 0$, $\hat{r} = 0.05$ and $w = 4.0$). (c) Same as (b), but plotted on a larger horizontal scale to more clearly demonstrate the behavior of the far-outer solution. (d) a nonmonotonic profile for sufficiently modest burned overpressures $p_b < T_c/f(0) - 1$ corresponding to a negative gradient at the material surface ($p_b = 10.0$, $\kappa^* = 0.2$, $\beta_c = 0.75$, $\alpha_s = 0.3$, $\phi = 1.0$, $\hat{r} = 0.05$ and $w = 2.0$). In (a) – (d), additional parameter values needed to calculate T_c were taken to be those used in Figure 6b with $M = 7.2$.

9. Gas velocity u_g in the solid/gas region $\xi < 0$. The three profiles correspond to the pressure profiles in Figures 8a, 8b-c and 8d, respectively.

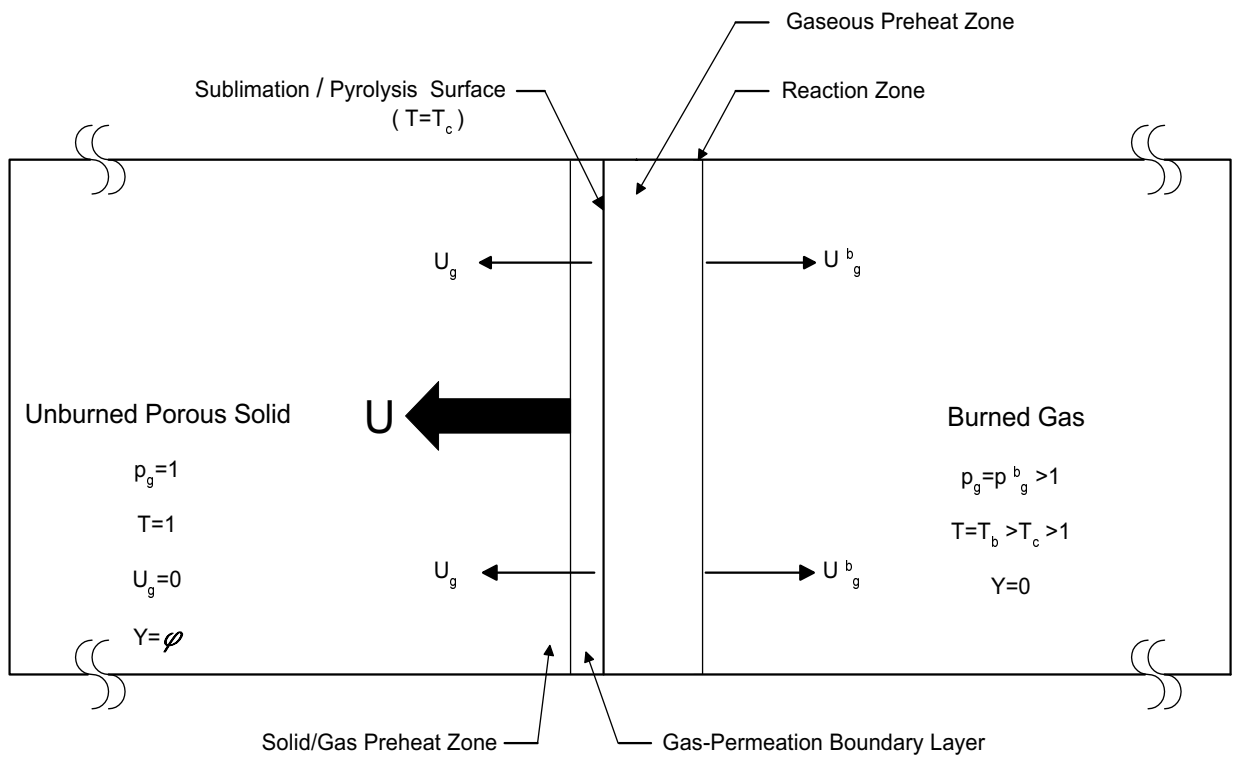


Figure 1

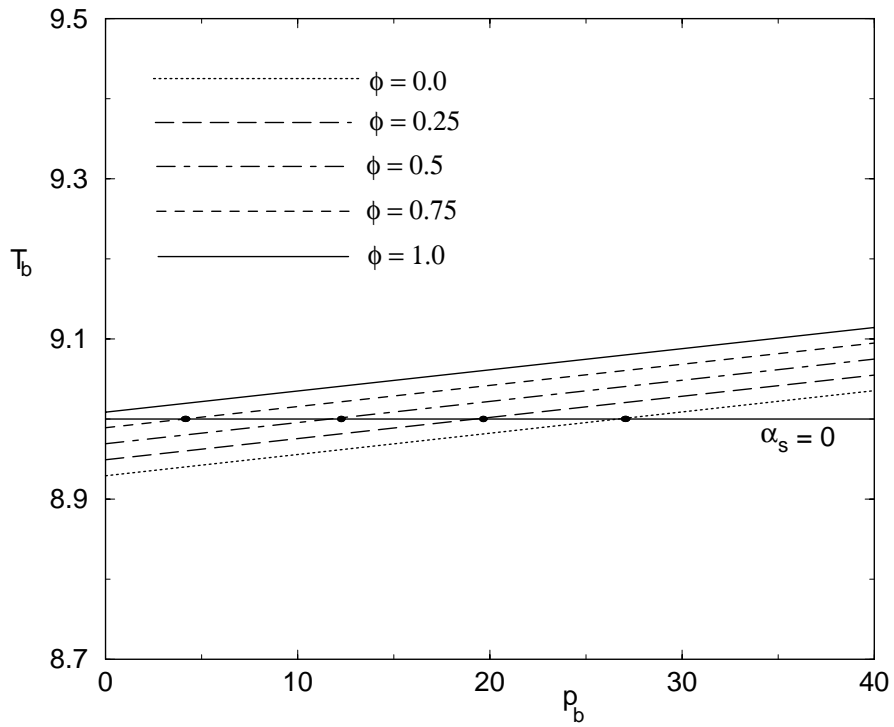


Figure 2a

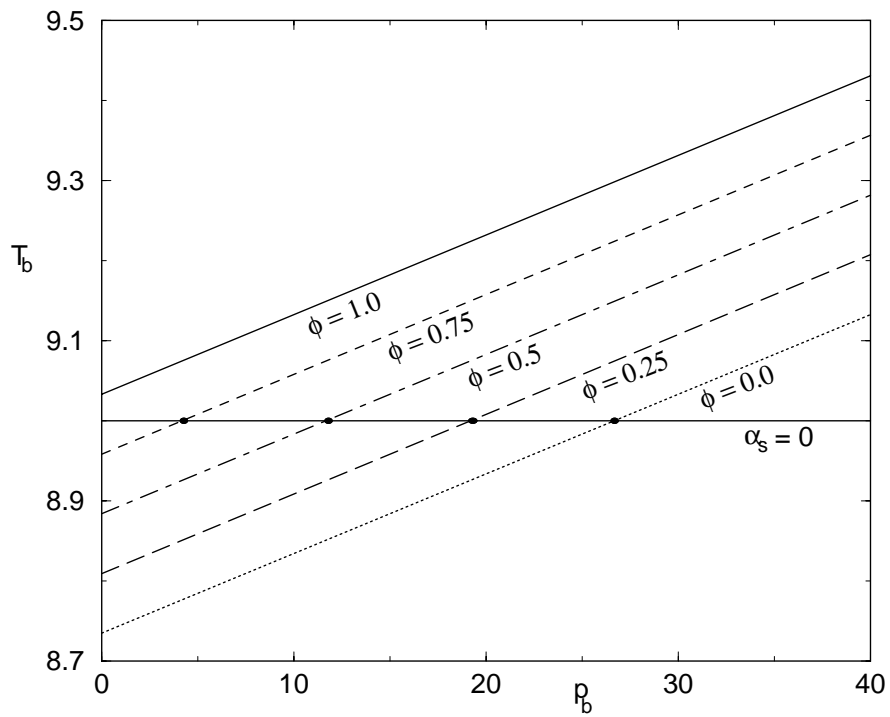


Figure 2b

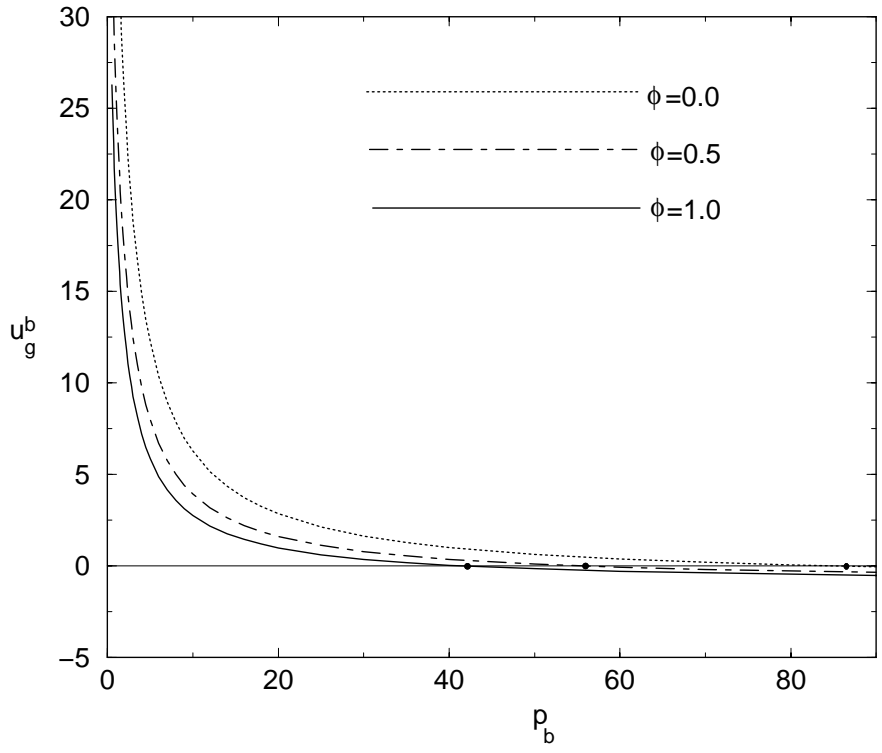


Figure 3a

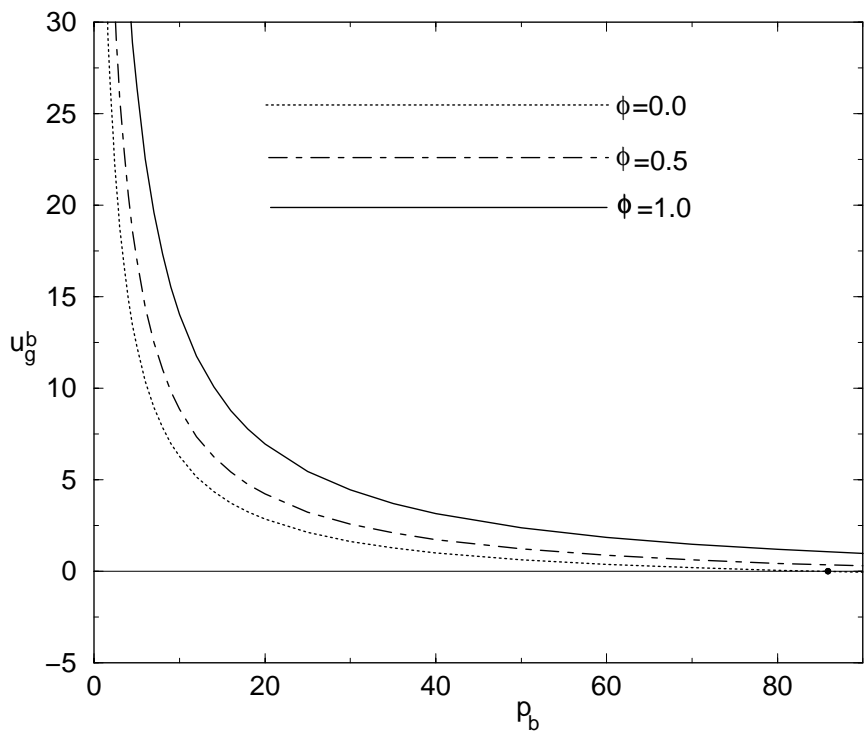


Figure 3b

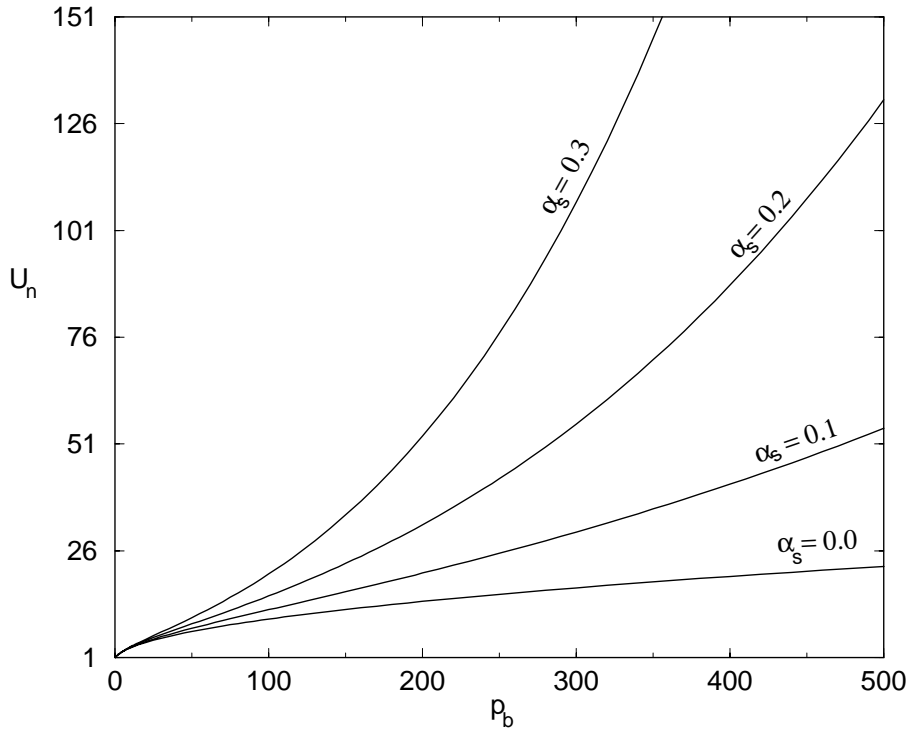


Figure 4

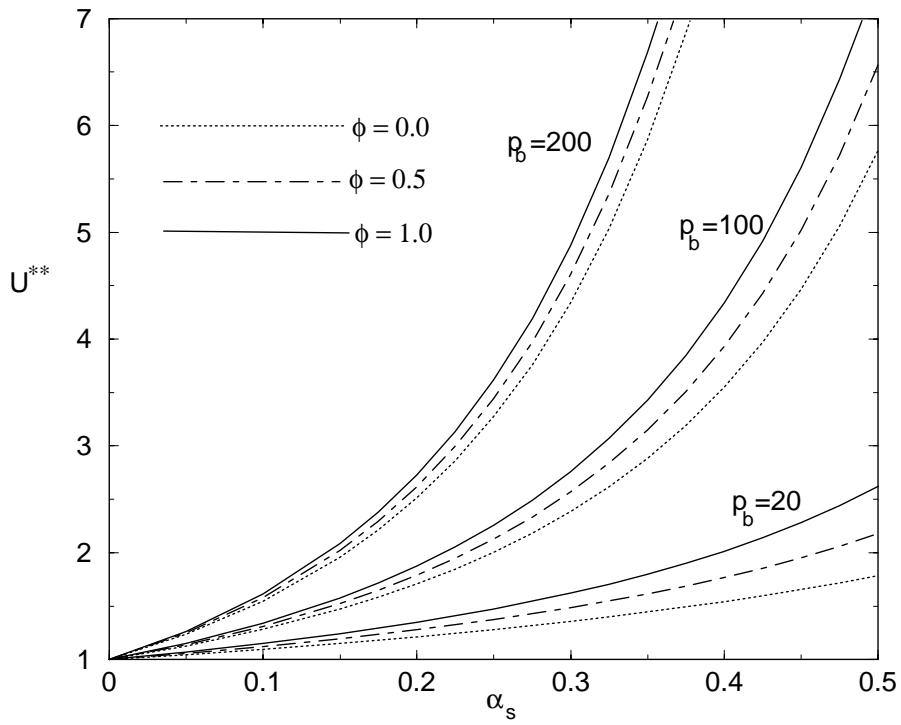


Figure 5

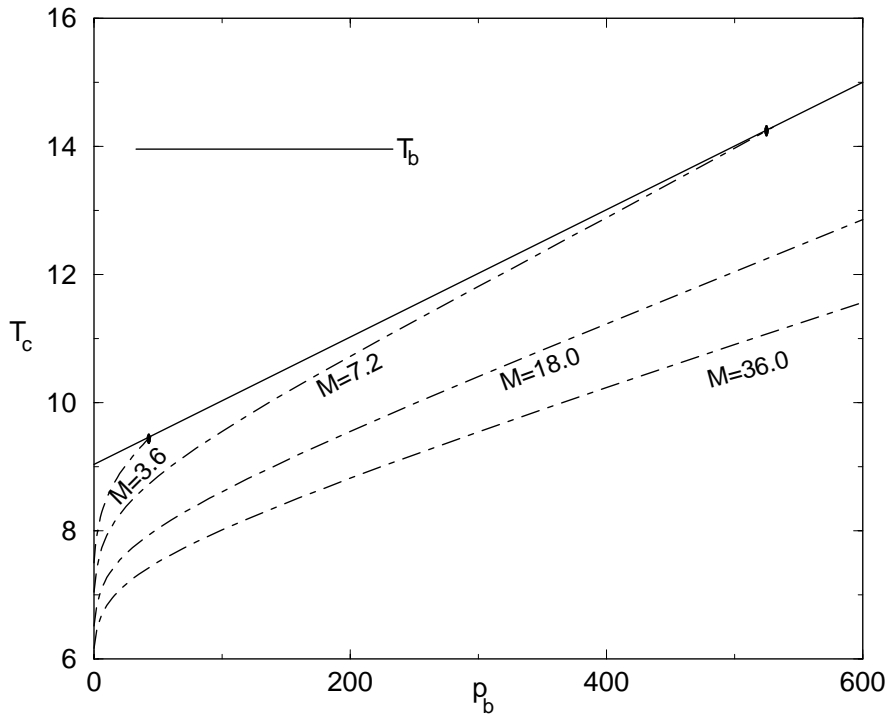


Figure 6a

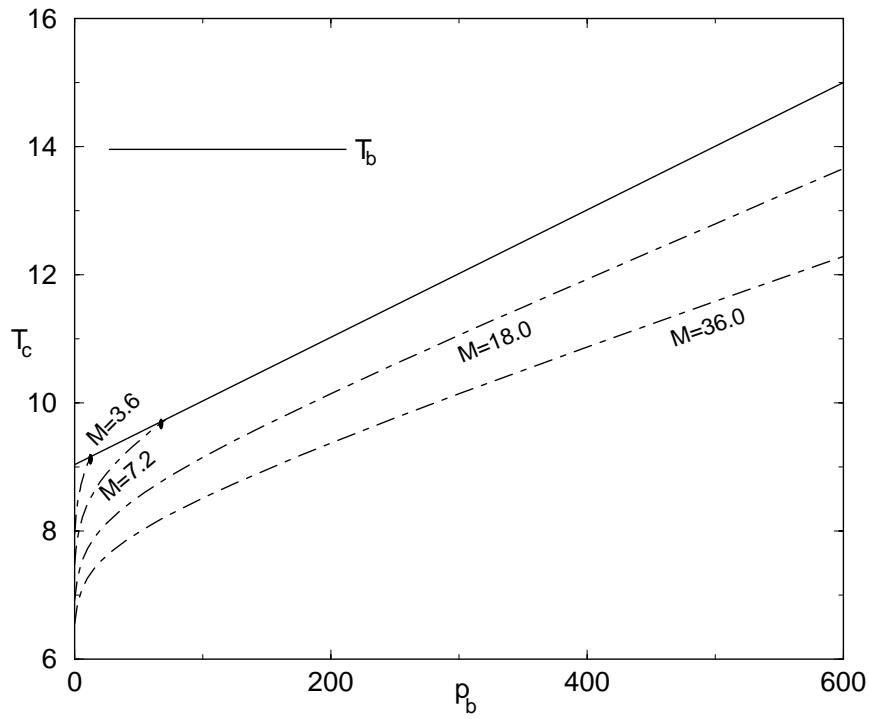


Figure 6b

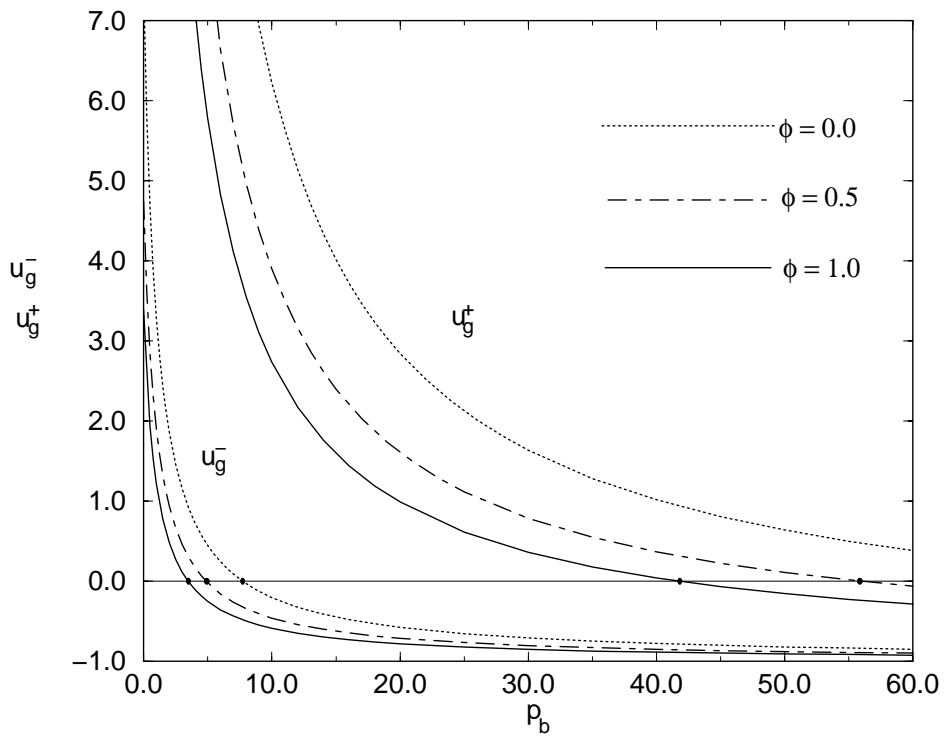


Figure 7

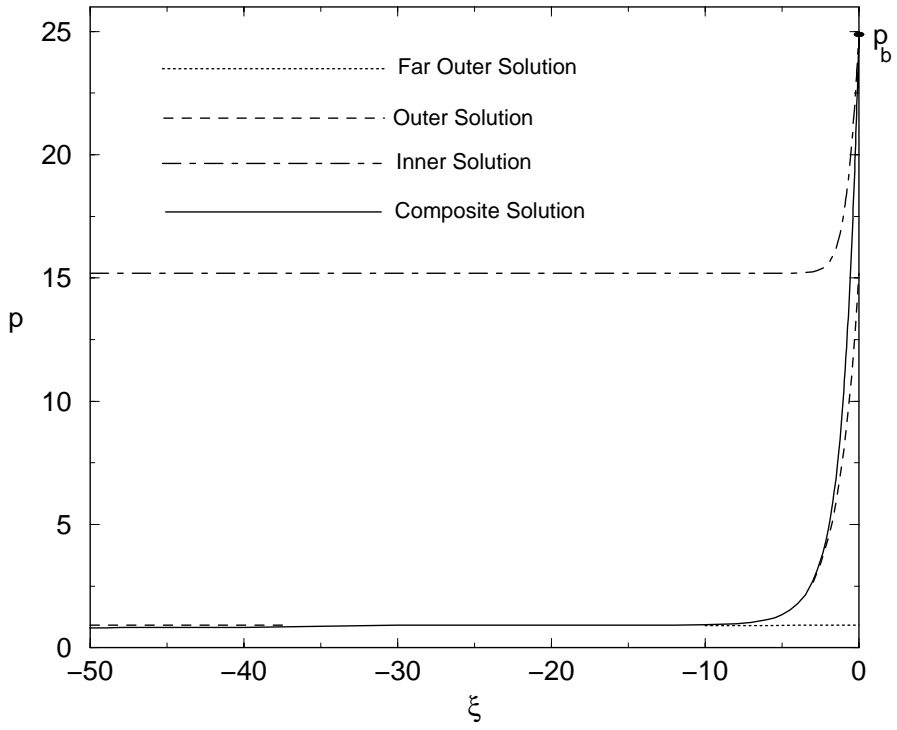


Figure 8a

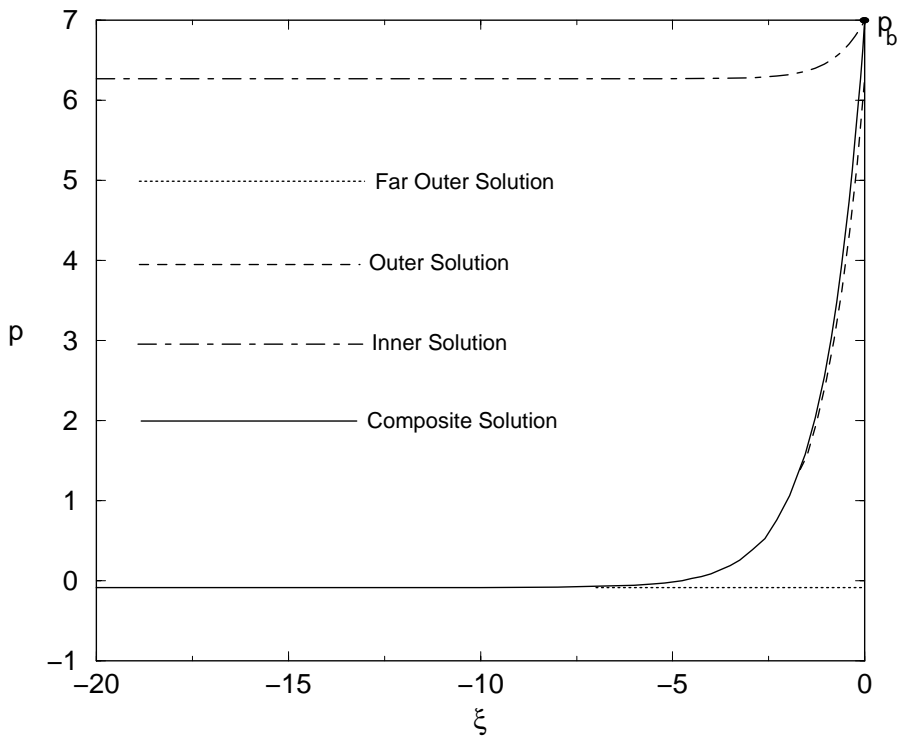


Figure 8b

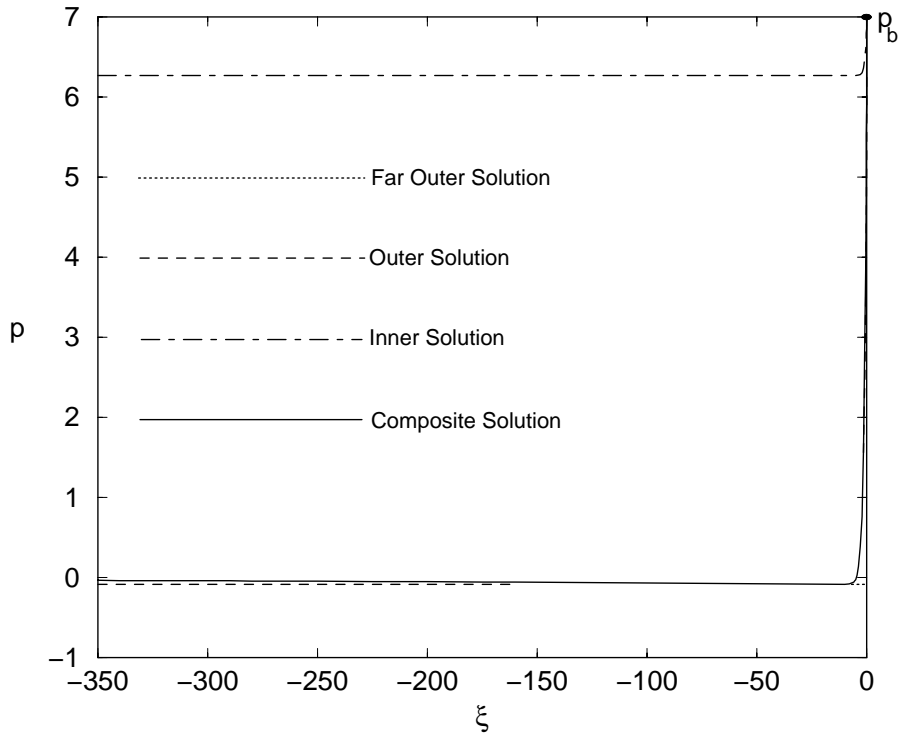


Figure 8c

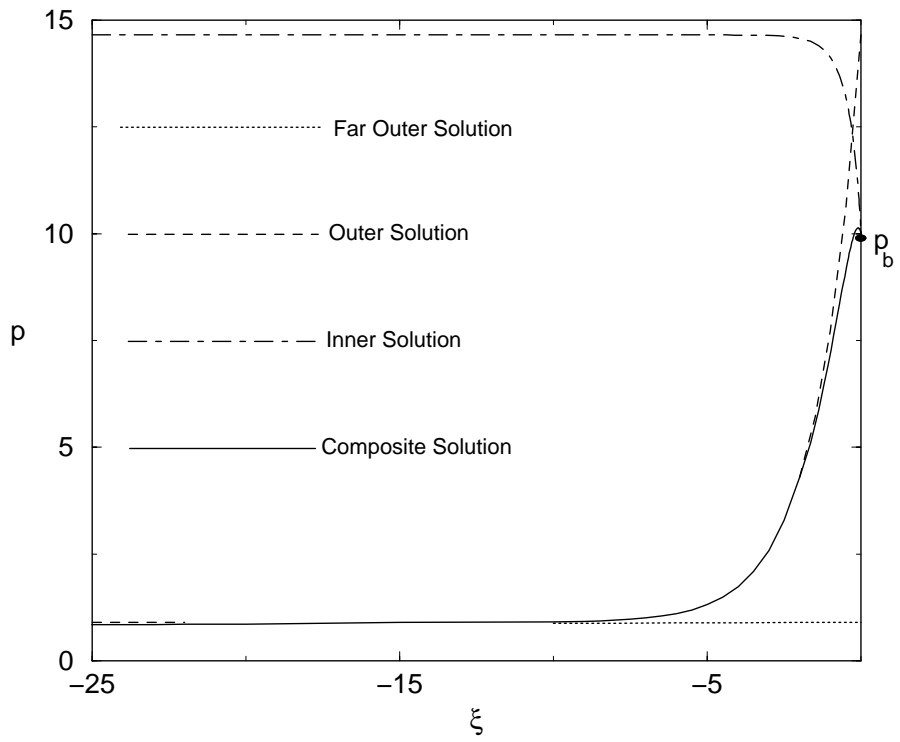


Figure 8d

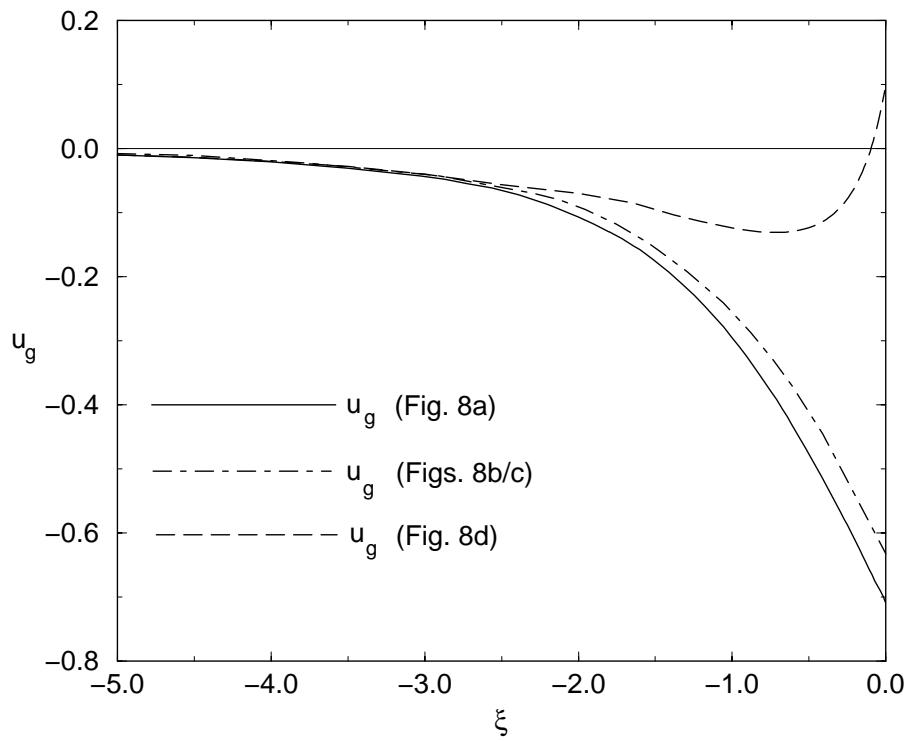


Figure 9